First posted online on 31 May 2019 as 10.1242/dev.180190
Access the most recent version at http://dev.biologists.org/lookup/doi/10.1242/dev.180190

NeuroMesodermal Progenitors (NMPs): a comparative study between Pluripotent Stem Cells and Embryo derived populations

Shlomit Edri[1, *], Penelope Hayward[1], Wajid Jawaid[2, 3, 4] and Alfonso Martinez Arias[1, *]

1. Department of Genetics, Downing Site, University of Cambridge, Cambridge, CB2 3EH, UK. 2. Wellcome Trust - Medical Research Council Cambridge Stem Cell Institute, University of Cambridge, Cambridge, UK. 3. Department of Haematology, Cambridge Institute for Medical Research, University of Cambridge, Cambridge CB2 0XY, UK.4. Department of Paediatric Surgery, Addenbrooke's Hospital, Cambridge University Hospitals NHS Foundation Trust, Cambridge, UK.

*Authors for correspondence
Shlomit Edri: se349@cam.ac.uk
Alfonso Martinez Arias: ama11@hermes.cam.ac.uk

Abstract

The mammalian embryos Caudal Lateral Epiblast (CLE) harbours bipotent progenitors, called Neural Mesodermal Progenitors (NMPs), that contribute to the spinal cord and the paraxial mesoderm throughout axial elongation. Here we performed a single cell analysis of different *in vitro* NMPs populations produced either from embryonic stem cells (ESCs) or epiblast stem cells (EpiSCs) and compared them to E8.25 CLE mouse embryos. In our analysis of this region our findings challenge the notion that NMPs can be defined by the exclusive coexpression of *Sox2* and *T* at mRNA level. We analyse the *in vitro* NMP-like populations using a purpose-built Support Vector Machine (SVM) based on the embryo CLE and use it as a classification model to compare the *in vivo* and *in vitro* populations. Our results show that NMP differentiation from ESCs, leads to heterogeneous progenitor populations with few NMP-like cells, as defined by the SVM algorithm, whereas starting with EpiSCs, yields a high proportion of cells with the embryo NMP signature. We find that the population from which the Epi-NMPs are derived in culture contains a node-like population, which leads to suggest that this population probably maintains the expression of *T in vitro* and thereby a source of NMPs. In conclusion, differentiation of EpiSCs into NMPs reproduces events *in vivo* and suggests a sequence of events for the emergence of the NMPs population.

Introduction

In mammalian embryos, the trunk consists of the endoderm, the spinal cord and the derivatives of different kinds of mesodermal (axial, paraxial, intermediate and lateral plate). Much of our current understanding regarding the development of this body region has focused on two progenitor cell populations: the node, that will give rise to the axial mesoderm (Beddington, 1982; McGrew et al., 2008; Tam and Beddington, 1987) and the Neural Mesodermal Progenitors (NMPs), a bipotent stem cell population that contributes to the spinal cord and the paraxial mesoderm (PXM) (Henrique et al., 2015; Selleck and Stern, 1991; Wilson et al., 2009). Both populations are closely related within the anterior region of the Caudal Epiblast (CE) in the embryo (Wymeersch et al., 2016). This association persists for as long as the node is visible, between stages E7.5 and E9.0 (Fig. 1, Fig. S1 and (Wymeersch et al., 2016; Wymeersch et al., 2019; Yamanaka et al., 2007). It is not clear when the NMPs arise but their association with the node suggests that they might emerge at the same time, around E7.5, from a multipotent population (Edri et al., 2019); the NMP population must then proliferate to sustain the axial extension process. Absence of the node results in severe axial truncations (Ang and Rossant, 1994; Davidson and Tam, 2000; Weinstein et al., 1994), suggesting a relationship between the node and the establishment and maintenance of the NMPs. However, little is known about these interactions.

The earliest identifiable NMPs emerge in the CE of E8.25 embryos distributed between the Node Streak Border (NSB) and the Caudal Lateral Epiblast (CLE) (Cambray and Wilson, 2007; Wymeersch et al., 2016; Wymeersch et al., 2019). They are associated with the coexpression of *T* (*Brachyury)*, *Sox2* and *NKx1-2* (Henrique et al., 2015; Steventon and Martinez Arias, 2017; Wilson et al., 2009). However, molecular analysis in embryos is limited, because of accessibility to primary material and the challenging temporal resolution. To circumvent these difficulties, over the last few years Embryonic Stem Cells (ESCs) have emerged as a useful model for mammalian development. In the context of axial extension, it has been possible to generate NMPs *in vitro* from Pluripotent Stem Cells (PSCs) (Edri et al., 2019; Gouti et al., 2014; Gouti et al., 2017; Lippmann et al., 2015; Tsakiridis and Wilson, 2015; Turner et al., 2014). These studies provide large quantities of material and allow the study of details that are difficult to obtain *in vivo*, particularly the structure and the genetic profile of the NMP population. In these studies, it is important to establish the relationship between the *in vitro* and the *in vivo* populations. A recent study aiming to do this and by using an ESCs based protocol, has established some features of an ESC derived NMP population (Gouti et al., 2017).

Here we perform a single cell analysis of different *in vitro* derived populations comparing them to those in the E8.25 embryo CLE (Ibarra-Soria et al., 2018; Pijuan-Sala et al., 2019), where NMPs can be clearly observed (Cambray and Wilson, 2007; Wymeersch et al., 2016; Wymeersch et al., 2019). We perform this analysis with a Support Vector Machine (SVM) based on the reference CLE embryo data. We use the SVM as a classification model to analyse the different *in vitro* NMP-like populations and show that while ESCs derived CLE-like populations are heterogeneous and contain few NMP-like cells, EpiSCs derived one, produce a high proportion of cells with the embryo NMP signature. Importantly we find that Epi-CE, the population from which the Epi-NMPs are derived (Edri et al., 2019), contains a node-like population and we show that this population can maintain the expression of *T* in vitro. Our results suggest a sequence of events for the NMPs emergence, which we discuss here.

Results

To understand the complexity and identity of the cell populations that emerge when recapitulating NMPs *in vitro* and how they relate to the embryo CLE, we characterized these populations at a single cell level. We focused our study on the populations that we have described in (Edri et al., 2019) and extracted mRNA from single cells of ES-NMP, (Edri et al., 2019; Turner et al., 2014), Epi-CE and Epi-NMP (Edri et al., 2019), as well as of the *T* expressing cells from the Epi-CE population (Epi-CE-T, Materials and Methods). As a

reference for the *in vivo* population, we used a gene expression data set containing 7,006 cells from E8.25 embryos (Ibarra-Soria et al., 2018; Pijuan-Sala et al., 2019). However, rather than using the complete data set, we performed an in silico dissection of the caudal region of the embryo (Fig.1). We selected cells coexpressing *Sox2* and *T* - putative NMPs (Cambray and Wilson, 2007; Henrique et al., 2015; Koch et al., 2017; Tsakiridis et al., 2014; Wymeersch et al., 2016; Wymeersch et al., 2019); cells that express *Sox2* and *Nkx1-2* but do not express *T* - preneural progenitors (Henrique et al., 2015; Schubert et al., 1995); and cells that express *T* but not *Sox2*, *Mixl1* or *Bmp4*, which represent mesodermal progenitors and exclude progenitors for the endoderm (*Mixl1*) and the allantois (*Bmp4)* (Dunty et al., 2014; Lawson et al., 1999; Robb et al., 2000; Wolfe and Downs, 2014). We refer to these three population as NMP, preNeuro and preMeso respectively. The extraction process yielded 498 cells that represent the caudal region of the embryo (108 NMP cells, 133 preNeuro cells and 257 preMeso cells).

In vitro derived populations reflect temporally overlapping embryonic populations

As a first step in our analysis we performed batch correction analysis between the embryo and the *in vitro* population datasets, based on the detection of mutual nearest neighbours (MNNs) in the high-dimensional expression space ((Haghverdi et al., 2018) and Fig. S2-S3).

For the batch corrected data we implemented Seurat package (Butler et al., 2018; Stuart et al., 2018) to observe how the cells clustered together (Materials and Methods). The number of clusters tested was between 2-8 and following the projected cells in tSNE plots coloured according to the conditions and clusters (Fig. 2A-B), Seven clusters were chosen for the downstream analysis. The marker genes that distinguish between clusters are shown in Fig. S4. The tSNE plots in Fig 2A-B allowed us to obtain a first approximation of the transcriptional complexity of the different samples. There is an overlap between the different NMP-like populations to themselves and to the cells from the embryo in the dimensionally reduced gene (Fig. 2B).

Fig. 2B revealed how each cluster relates to the different samples. Cluster 3 is composed mainly from Epi-CE-T, cluster 5 from ES-NMP and cluster 6 from E8.25 and Epi-CE-T. Using the major reference genes of the CLE gene expression signature (Fig.1, Fig. 2C and Fig. S5), we observe a spread in the markers expressed by the different populations which can be used to determine their identity. Cluster 5 contains cells that express pluripotent markers (*Nanog*, *Rex1* also known as *Zfp42*, *Sox2*, *Esrrb*, *Fgf4*) whereas cluster 3 exhibit cells with node identity (*T*, *Foxa2*, *Nog*, *Chrd*, *Shh*) and cluster 6 cells that express mesodermal markers (*Tbx6*, *Cited1*, *Msx1* and *Msx2*), the range of *Hox* genes (*Hox1-Hox9*) and CE markers (*Wnt3a*, *Fgf8*, *Cdx2*, *Cdx4*, *Cyp26a1*). Clusters 0-2, are composed from cells belonging to the ES-NMP, Epi-CE, Epi-CE-T and Epi-NMP population, and exhibit some similarity to the gene expression profile of cluster 6.

Analysis of the gene expression patterns associated with each cluster (Fig. 2C and Fig. S5), revealed the heterogeneity of these populations, particularly in the ES-NMP sample, where we can find cells with a mixed signature of pluripotency (*Nanog*, *Rex1*, *Sox2*, *Esrrb*, *Fgf4*), primed epiblast (*Fgf5*, *Otx2* and *Cdh1*), a later epiblast population that expresses some CLE and NMP markers as well as cells with a neural identity and others with mixed mesodermal characteristic. Overlapping with the last population, we notice a group of cells with mixed potential expressing *Mixl1* and *Fgf17* together with *Evx1, Hoxb9*, *Oct4* (also known as *Pou5f1*) and Wnt genes which might represent the posterior primitive streak population that will give rise to mesendodermal tissue (Dunty et al., 2014; Kojima et al., 2014; Robb et al., 2000; Wolfe and Downs, 2014).The heterogeneity of the ES-NMPs confirms the conclusion from our previous ensemble study (Edri et al., 2019) that differentiation in the absence of FGF leads to a highly heterogeneous and asynchronous populations with some but few NMPs.

The Epi-NMP population is enriched in cells with expression profiles clearly associated with E8.25/8.5 embryo - expression of *Cyp26a1* and *Cdh2*- and absence of *Otx2*, *Oct4, Cdh1* and *Fst*, all of which are associated with earlier stages of the embryo (E7.5, Fig. 2C and compare gene expression of E8.25 CLE embryo to Epi-NMP in Fig. S5). *In vitro*, Epi-NMPs are derived from Epi-CEs (Materials and Methods and (Edri et al., 2019)) which can explain how the expression of the different genes indicate a progress in the developmental stage from Epi-CE to Epi-NMP (early epiblast markers in Epi-CE versus CLE markers in Epi-NMP, Fig. S5). We also observe that Epi-NMPs, but not Epi-CE, contains a few cells differentiated into mesoderm as highlighted by the expression of *Tbx6, Meox1* and *Aldh1a2* (Fig. S5). Most surprisingly, we notice that the Epi-CE population, but not Epi-NMP, contains cells coexpressing genes associated with the node *e.g. Nodal*, *Foxa2*, *Ccno, Chrd, Nog and Shh* (Fig. S5). A similar population can also be found in the Epi-CE-T and suggests the presence of node-like cells in the Epi-CE population. These cells are very reduced in the Epi-NMP population, following the characteristic of the E8.5 CLE (Fig. 1).

The above observations provide support for our conjecture that that Epi-CE and Epi-NMP correspond to temporally consecutive populations in the embryo, which probably reflect a spectrum between E7.5 (emergence of the node (Davidson and Tam, 2000), Epi-CE) and E8.25/8.5 (Epi-NMP), when NMPs are clearly discernible (Wymeersch et al., 2016; Wymeersch et al., 2019). The temporal sequence can also be observed in the pattern of *Hox* genes expression as the Epi-NMP population expresses more posterior *Hox* genes than the Epi-CE (Fig. S5)

The NMP landscape in the E8.25 embryo

To interpret the *in vitro* derived cell populations, we used the caudal cells dissected in silico from the E8.25 embryo to build an SVM pipeline that would enable us to map the NMP-like cells to the *in vivo* CLE. As a first step, we attempted to identify phenotypically distinct populations amidst the three pools of cells that we had defined based on their pattern of *T*, *Sox2* and *Nkx1-2* expression (Fig. 3A). After processing the single cell data, for both the embryo and the *in vitro* samples, we found a total of 14,822 genes that can be used for the analysis (Materials and Methods). To provide identifier genes associated with the CLE region, we based our gene selection on the report from Koch et al. 2017, in which the authors perform an ensemble analysis of the caudal region of the E8.5 embryo based on the levels of *Sox2* and *T*. This work identified 1,402 genes that, together, provide specific signatures for five distinct subpopulations in the caudal end of the embryo: Group 1: axial elongation and trunk development; Group 2: early mesoderm, Group 3: later (committed) mesoderm, Group 4: early neural and Group 5: later (committed) neural ((Koch et al., 2017) and Table S3).

In this study, the marker genes of Group 1 are significant in cells that are positive for *Sox2* and *T* and are hence defined as putative NMPs. Moreover, these cells also have significant expression of marker genes from Groups 2 and 4, which are upregulated in cells that are defined as early mesoderm (Group 2) and early neural (Group 4). We used these 1,402 genes and add to them 69 genes which expressed in the decision-making region of the embryo according to the literature (Table S1 and (Edri et al., 2019)), yielding 1,471 genes which were reduced to 1,342 after removal of genes whose mean expression is zero (Table S2). These 1,342 genes were used to cluster the embryo data using a SC3 R package (Kiselev et al., 2017), an algorithm based on k-means clustering (Materials and Methods).

The analysis yielded an optimal number of four clusters in the E8.25 cells (Fig. 3A, Materials and Methods) and 96 marker genes that act as discriminating identifiers of the clusters (Table S3). The top ten marker genes associated with each cluster are visualized in Fig. 3A. Having allocated cells to the 4 clusters based on their gene expression, we looked to see how each of the three functional groups (NMPs candidates, preNeuro and preMeso) that compose the CLE region, occupies each of the clusters.

Cluster 1 is a mixed cluster, composed of the three cells categories: NMP candidates, preMeso and preNeuro (Fig. 3A and Table S3); 71% of its 28 marker genes are part of the NMP profile gathered from the literature, including *Cdx4*, *Nkx1-2*, *Fgf8* and *Fgf17* (Fig. 3A, Table S3 and (Koch et al., 2017)). Cluster 2 is mainly composed from cells defined as preMeso and the most highly expressed genes in this cluster exhibit a mesodermal affiliation (lateral plate mesoderm (LPM), intermediate mesoderm (IM), PXM and somites, see Table S1) with 91% of the 23 marker genes being mesodermal according to (Koch et al., 2017) (Fig. 3A and Table S3). Cluster 3 is constructed mostly from preNeuro cells and has a neural identity characterized by genes related to the spinal cord and the nervous system. 85% of the 13 marker genes of cluster 3 defined as neural based on the report of (Koch et al., 2017) (Fig. 3A and Table S3). Finally, cluster 4 is mostly composed of preMeso cells and, as defined in Koch et al. 2017, 34% of the 32 marker genes match to Group 3 (LPM and IM) but with additional genes affiliated to endoderm and IM (Table S1 and Table S3).

Our clustering suggests that cluster 1 has an NMP signature since it highlights genes like *Nkx1-2*, *Cdx1-4*, *Fgf8, Grsf1*, *Epha5* and *Cystm1*, all associated with NMPs (Cambray and Wilson, 2007; Edri et al., 2019; Gouti et al., 2014; Gouti et al., 2017; Henrique et al., 2015; Koch et al., 2017; Wymeersch et al., 2016; Wymeersch et al., 2019). Furthermore, it suggests that rather thasn being a population of bipotent cells characterized mainly by the coexpression of *Sox2* and *T* at the mRNA level, which makes only 29% of cluster 1, the ensemble appears to contain some pre-mesodermal (38%) and pre-neural (33%) cells. This analysis thus raises a question about the differences between the preMeso and preNeuro cells in cluster 1 in comparison to those that are found in clusters 2 and 3. One probable explanation is that cluster 1 encompasses very early neural and mesodermal cells, embedded in the NMP region of the mouse embryo, whereas the others clusters contain committed cells, similarly to what was found in Koch et al. 2017. Indeed, cluster 1 includes genes that have been previously linked to the NMP profile together with genes that have neural or mesodermal characteristics. Based on the work of Koch et al. 2017 out of the 28 marker genes defining cluster 1, two genes (*Ptk7* and *Fgf8*) are linked to Group 1 (axial elongation and trunk development); 15 genes (*Epha5*, *Nkx1-2*, *Cdx,2,4*, *Cystm1*, *Acot7*, *Stmn2*, *Fgf17*, *Lhpp*, *Mgst1*, *Lix1*, *Hoxc4*, *Ccnjl*, *Sp8* and *Oat*) are linked to Group 4 (early neural) and the rest of the genes are either expressed in the embryo CLE at around E8.5 (*Grsf1*, *Cdx1*, *Hoxb9*, *Hoxc9*, *Wnt5b)*, exhibit neural (*Hes3*, *Ncam1*, *Pmaip1*) or mesodermal (*Evx1*, *Hes7*, *Foxb1* which also express in the neural plate) progenitors characteristic (see Table S1 for references).

Having identified a gene based structure for the E8.25 CLE embryo the next step was to build an SVM classifier that would learn the gene profile of the 4 different clusters found in the embryo data. After testing its performance and its stability on the embryo (Fig. 3B, Materials and Methods), the SVM was used to assign cells of the *in vitro* populations to the 4 classes (clusters) based on their gene expression.

To build a robust and accurate classifier selecting the input features (genes) that the SVM needs to learn was an important task. Hence, we first wanted to identify the informative genes associated with the 4 clusters. To do this and to avoid the underrepresentation of genes that were not previously linked to the NMPs, we used the whole set of qualified genes (14,822). The selection of the genes was done by computing the MI between the genes and the 4 clusters (Materials and Methods, Table 4), which resulted in 82 informative genes that were used as features input to the SVM. The feature selection process leads to a classifier that by reading the expression of these 82 genes can correctly classify 97% of the input cells (Fig. 3B, Table 4). 60% of the 82 informative genes are identical to the 96 marker genes of the 4 clusters, whereas 40% of the genes include genes like *T*, *Hoxc8*, *Hoxb8*, *Cdkn1c*, which are expressed in the embryo CLE at E8.25/8.5.

A comparison between the *in vitro* and *in vivo* cell populations

We used the SVM established from the embryo data to explore the structure and nature of the *in vitro* populations. To do this, we first needed to ensure that the input cells from the *in vitro* populations, did not contain cells with gene expression patterns which the SVM had not been trained on, as we only want to test the cells with similarity to the E8.25 caudal region (Fig. 3A and step 1 in Fig. 4A). Similarly to the in silico dissection of the CLE from the embryo cells, we selected cells coexpressing *Sox2* and *T*; cells expressing *Sox2* and *Nkx1-2* but not *T* and cells expressing *T* but not *Sox2*, *Mixl1* or *Bmp4*. This step resulted in filtering out a higher number of cells from the ES-NMP condition (45%) in comparison to the other conditions (~30%), consistent with the previously noted heterogeneity. Feeding the remaining CLE-like cells to the classifier with the expression of the 82 informative genes, which are the features the SVM had been trained on and needs to perform the classification task, resulted in the assignment of probabilities for each cell to be classified to each of the 4 classes (Fig. 4A). Since the true classification of the *in vitro* cells is not known and since there might be some hidden classes in the *in vitro* populations that were not trained using the embryo data, only the cells with minimum probability of 0.8 are assigned to the class with the highest probability amongst the 4 classes and proceeded to the next step (see the probability plot under Step 6 in Fig. 4A: probability of 0.8 is indicated by the red line, see also Materials and Methods). Again, in this step the highest filter of cells (50%) was observed in the ES-NMP condition compared to the others (~30-35%), suggesting that this condition produce high quantity of cells that do not correspond to the E8.25 embryo CLE. The last step (step 7 Fig. 4A) was to summarize the distribution of the cells of each sample across the 4 classes. Most of the qualified cells (Fig. 4A, Table of step 6) from ES-NMP (84%) and Epi-NMP (73%) were allocated to class 1 (step 7 Fig. 4A), which is associated with the NMPs signature. On the other hand, more than 90% of the qualified cells (Fig. 4A, Table of step 6) from Epi-CE (91%) and Epi-CE-T (97%) were classified to class 4 (step 7 Fig. 4A), which is characterized by the expression of mesodermal and endodermal genes. Class 2 and class 3, which have mesodermal and neural differentiation characteristics, did not attract many cells from the different samples suggesting that the *in vitro* cells, passed through this pipeline, are not very differentiated.

Figure 4B shows the average expression of the 96 marker genes of the 4 clusters in the *in vitro* cell populations. This result emphasizes that the same classes from different samples clustered together, which displays the similarity of the cells from different conditions assigning to the same class. In addition, it shows that the *in vitro* cells exhibit the expression of marker genes for the 4 classes found in the embryo, demonstrating that the SVM pipeline detects the *in vitro* cells in agreement with the learned embryo cells.

A node-like population induced *in vitro*

The finding that Epi-CE and Epi-CE-T, classified mainly to class 4 and that Epi-CE is the origin of Epi-NMP (Materials and Methods, (Edri et al., 2019)) led us to investigate further the identity of cluster 4. As a first step, we arranged all the qualified cells out of the SVM pipeline (Fig. 4A, Table of step 6) into a pseudotime ordering using TSCAN, a Biocounductor R package version 1.16.0, (Ji and Ji, 2017) (Materials and Methods). This analysis revealed that class 4 cells (red cells in Fig. 5A) are split into 2 pseudotime ranges, with class 1 cells (blue cells in Fig. 5A) forming a bridge between these two classes. This result lends support to the possibility that Epi-NMP cells (mainly classified to class 1) are derived from Epi-CE (class 4 mainly composed from Epi-CE and Epi-CE-T). It also raises the existence of two different populations in Epi-CE. When exploring the highly expressed genes that define the 2 pseudotime ranges of class 4 (Fig. 5A, Materials and Methods and Table S5), we observed that the later range is defined by genes associated with rapidly dividing cells, whereas the early one doesn't show this enrichment (Fig. 5A). This observation suggests the existence, in class 4, of a group of cells in a phase of large expansion. Similar results were obtained by pseudotime ordering the cells using Monocle (Fig. S7), a Biocounductor R package version

2.10.1 (Qiu et al., 2017a; Qiu et al., 2017b; Trapnell et al., 2014), where class 4 is divided to 2 groups: an early one that contains Epi-CE-T cells and a later one mainly composed from Epi-CE. Class 1, which is composed from Epi-NMP and ES-NMP, are a later population in the pseudotime range, in comparison to class 4 (Epi-CE conditions). This result indicates that class 1 is derived from class 4, which is true in culture (Epi-NMP derived from Epi-CE) and in the embryo: the CE will harbour the NMP in a later state.

The presence of endodermal and mesodermal markers in class 4 is surprising as it suggests the existence of a cell type in the embryo caudal region, that would be associated with these germ layers. One structure that could fit this criterion is the node (Blum et al., 2007; Lee and Anderson, 2008; Martinez Arias and Steventon, 2018), a structure that appears at E7.5, contains the progenitors of the axial mesoderm (Beddington, 1982; McGrew et al., 2008; Tam and Beddington, 1987) and has been associated with the NMPs (Albors and Storey, 2016; Garriock et al., 2015; Henrique et al., 2015; Wymeersch et al., 2016). Thus, we considered the possibility that class 4 contains node cells.

At a very coarse level, the node can be identified as cells expressing combinations of three genes; *Foxa2*, *Nodal* and *T* (Fig. 5B (Davidson and Tam, 2000; Jeong and Epstein, 2003a; Lee and Anderson, 2008; Shiratori and Hamada, 2006)). Applying this coarse definition, we detected node-like cells in our *in vitro* samples with a very high representation in class 4 (Fig.). The allocation of a node identity to cells in class 4 is not a bias of the sample size, as a statistical test controlling the size of the classes yielded that class 4 has the highest proportion of node-like cells is statistically significant ($p - value < 0.001$, Materials and Methods). To further test this coarse identification of node-like cells, we gathered a list of additional genes associated with the structure and function of the node *e.g. Shh*, *Ccno* and *Chrd* (Davidson and Tam, 2000; Funk et al., 2015; Jeong and Epstein, 2003a; Lee and Anderson, 2008; Shiratori and Hamada, 2006; Tam and Behringer, 1997) and tested for their expression in class 4 as can be seen in Figure 5D.

Having identified node-like cells in our *in vitro* populations we thought we could use the dynamic changes in this region of the embryo to stage our *in vitro* populations. For example, at the time of its appearance the node expresses *Oct4* and *Otx2* however by E8.0-8.5 the expression of these genes have disappeared from the node (Cajal et al., 2012; Downs, 2008). The expression of *Oct4* is particularly diagnostic for this transition.

Moreover, we checked the proportion of the node-like cells in the 2 pseusotime ranges of class 4, as shown in Table 1, however no difference was found. This result, supports our hypothesis that these two populations are very similar, however one of them represents an amplifying population versus the second one which is more stable in terms of size.

In the in silco E8.25 embryo CLE we found 38 node-like cells (Fig. 6A-B), 30 of which were mapped to the embryo class 4 (Fig. 6A). When comparing the node-like cells in class 4 of the embryo to those of the *in vitro* cells, some notable differences become apparent (Fig. 6B). For example *Oct4*, which is off in the embryo cells. Since Epi-NMPs express very few node genes (Fig. 4A step 7 and Fig. 6C) and no *Oct4*, first supports our previous assertion that it has the closest relationship to the E8.25 CLE region, second that the node-like cells are lost in the transition between Epi-CE and Epi-NMP (Fig. 6C) and that the Epi-CE cells represent a developmentally earlier cell state than the Epi-NMPs.

An *in vitro* functional test of the *in vitro* induced node-like population

Previously we showed that the Epi-NMP population has a limited but clear self renewing ability in culture when exposed to FGF and Chiron (Edri et al., 2019). These cells maintain *T* and *Sox2* expression for at least two passages (Epi-NMP, Epi-meso2, Epi-meso3…) though, over time, the levels of NMP markers go down and the cells exhibit a slow increase in the expression of differentiation genes associated with neural fates (Edri et al., 2019). In the embryo, the self renewing population also decreases with time and this is associated with the node disappearance (Steventon and Martinez Arias, 2017; Wymeersch et al., 2016). Thus, we considered that, in our *in vitro* system, the loss of *T* might be associated with the

loss of node-like cells. To test this, we added node-like cells from Epi-CE to Epi-NMP and passaged the mixed sample to make Epi-meso2, then we checked whether the addition of node-like cells could maintain the levels of *T* expression.

The experiment is described in Figure 6d: as a source of NMP-like cells we used a Ubiquitin::tomato cell line and as a source of node cells, a Nodal::YFP cell line. Both were cultured to produce Epi-CE: Epi-CE RFP (from Ubiquitin::tomato cell line) and Epi-CE Nodal (from Nodal::YFP cell line). The Epi-CE RFP were further grown to make Epi-NMP (Epi-NMP RFP). After two days of culturing Epi-NMP RFP, we plated a mixture that equally consists of Epi-NMP RFP positive cells and Epi-CE Nodal positive YFP cells (Fig. 6D, Fig. S8A-B, Materials and Methods). The mixture (Epi-meso2) was cultured for 4 days (Fig. 6D) until sorting the cells to RFP positive (sample named: EM2-RFP+4d, contains only the Ubiquitin::tomato cells) and RFP negative (sample named: EM2-RFP-4d, contains Nodal::YFP cells and might contain Ubiquitin::tomato cells that didn't express RFP, Fig. S8C and Materials and Methods). These populations of cells were compared to the EM2-RFP4d, which are only Epi-NMP RFP cells cultured for 4 days to make Epi-meso2 (Fig. 6D, Materials and Methods).

Addition of node-like cells to the Epi-NMP population elevates the level of *T* and *Foxa2*, maintains the expression of *Cdx2* and *Nkx1-2* and decreases the level of neural fate markers: *Sox2* and *Sox1* (Figure 6E and Figure S9 EM2-RFP4d versus EM2-RFP+4d). In addition, there is no much difference in the expression of *Tbx6, Hoxc6, Fgf8* and *Cyp26a1*, when comparing those genes between EM2-RFP4d and EM2-RFP+4d.

This result, aligned with what we previously showed (Edri et al., 2019), suggests that node-like cells are necessary to maintain the relative levels of *Sox2* and *T* and buffer the tendency that the Epi-NMPs have towards the neural fate when passaging them in culture.

Discussion

Over the last few years, ESCs have emerged as a useful experimental system to study mammalian development. While they are no substitute for the embryo, they have some advantages when addressing processes that happen early in development, when material and experimental accessibility are scarce. However, their validation as an experimental system depends on testing how the events observed in culture relate to those taking place in the embryo. Here we have used mouse PSCs to analyse, at the single cell level, the origin and structure of NMPs, a bipotent population that is thought to give rise to the spinal cord and the paraxial mesoderm. As an important reference for our study we have used a single cell data set from E8.25 embryos, the stage at which NMPs are first distinguishable.

Analysis of NMPs derived from PSCs suggests that different protocols produce heterogeneous populations in terms of gene expression (Edri et al., 2019). To gain insights into these heterogeneities and their origins, we have performed a single cell transcriptomics analysis of the different populations. As a reference, we have used data from E8.25 embryos out of which we have dissected in silico the CLE/NSB region based on *T*, *Sox2* and *Nkx1-2* expression patterns, as cells that express these genes are often identified as NMPs. Our results suggest that, by this stage, these cells are distinct from those in the pluripotent epiblast. The transition between the states appears to be associated with the loss of expression of *Cdh1*, *Oct4*, *Fst* and *Otx2* and the gain of expression of *Cdh2* and *Cyp26a1* amongst others (Fig.1 and Fig.S1). Our results contrast with those of a recent study which allocated expression of *Cdh1* and *Oct4* to NMPs at E8.5 (Gouti et al., 2017). Analysis of published gene expression patterns (Fig.1, Fig.S1 and Table S1) supports our conclusions that these markers are associated with the pluripotent epiblast. It might be that changes in the transcription of these genes happens abruptly at around E8.25 and that there is a difficulty in staging the embryos. The transition from pluripotent epiblast to the bipotent cells in the CLE/NSB region can be detected in our vitro samples as represented by the transition from Epi-CE to Epi-NMP (Fig. 2 and Fig. S5 and see also Edri et al 2019).

As a reference for the *in vitro* derived populations, we used a clustering algorithm on existing datasets (Ibarra-Soria et al., 2018; Pijuan-Sala et al., 2019). to classify populations in the embryo: class 1 with NMP signature; class 2 with mesodermal signature; class 3 with neural signature and class 4 with extraembryonic, endoderm and IM signature. Class 1 contains cells coexpressing *Sox2* and *T* and cells in a pre neural or mesodermal state, *i.e.* not all of them coexpress exclusively *Sox2* and *T*. This observation emphasizes the notion that the coexpression of *Sox2* and *T* alone is not a valid definition, or at least it is not an absolute structural condition, for NMPs (see also (Edri et al., 2019)). It also raises the possibility that an NMP population is not only a collection of *Sox2* and *T* coexpressing cells (Gouti et al., 2014; Gouti et al., 2017; Turner et al., 2014), but includes a heterogeneous population of mesodermal and neural poised and early differentiated cells. This situation is reminiscent of many stem and progenitor cell populations and suggests that, as in some of those cases (Huang, 2009; Moris et al., 2016; Pina et al., 2012), these different cell populations are in dynamic equilibrium. A suggestion has been made that differentiation from the *T*/*Sox2* expressing population is a stochastic event biased by cell signalling (Gouti et al., 2017), our results support that observation but also suggest that the NMP population includes differentiation poised cells.

The structure of the E8.25 caudal region inferred from our analysis was used as a reference for the study of the *in vitro* derived populations. To do this, we used the four classes derived from the embryo data to build an SVM classification model that allowed us to allocate cells from the different protocols to our reference. We find that the ESC based protocol contains few cells allocated to the E8.25 embryo CLE, but that the EpiSCs samples are enriched. Furthermore, we find that Epi-NMP cells, which are derived from Epi-CE (Materials and Methods) contain the most E8.25 CLE-like cells (>70% of the selected cells, Fig. 4A) and most of them map to class 1. Furthermore, we find many E8.25 CLE-like cells in the Epi-CE population (>60% of the selected cells, Fig. 4A), but in contrast with Epi-NMPs, these cells predominantly map to class 4. Interestingly, very few cells of the Epi-CE descendant, Epi-NMP, map to class 4. A detailed analysis of class 4 reveals that it has a large representation of node-like cells and, interestingly, of the floor plate. The floor plate in the embryo shares many features with the node and its main derivative, the notochord. This allocation is confirmed by the identification of node-like cells in the embryo reference data.

The representation of cells from two different sequentially induced *in vitro* populations to one embryonic stage is, at first sight surprising, however we believe that there is an explanation. The CLE at E8.25 is derived from an earlier caudal region, at E7.5, whose most prominent feature is the node, that is maintained until E9.0. Thus, at E8.25 the embryo does have a signature of an early stage in the node. The representation of node cells in Epi-CE but not much in its progeny, Epi-NMP, suggests that, in adherent culture the conditions are not conducive to the maintenance of the node. What we find interesting, given the relationship between Epi-CE and Epi-NMP, is the presence of NMP-like cells in the Epi-NMP population. This lead us to speculate that in the embryo there might be a very close relationship between the emergence of the node and of the NMPs, something that has been suggested before (Albors and Storey, 2016; Garriock et al., 2015; Henrique et al., 2015; Wymeersch et al., 2016; Wymeersch et al., 2019).

We find two interesting features of the possible relationship between these two populations. The first one is the observation that within the Epi-CE population there is a subpopulation in a high proliferative state and second, that there appears to be a relationship between a node population and the maintenance of the *T* and *Sox2* expression ratio. These observations led us to suggest that, in the embryo, NMP population arise early in development, near the node and that the node might play a role in its maintenance and amplification at that early stage. A need for amplification of the initial NMPs pool could be likely explained by the size of the primordia relatively to the size of the tissue that needs to be generated. It is not clear how the node would mediate this function but an interaction between BMP and Nodal (Edri et al.,

2019) might be important. A relationship between the node and axial elongation can be gauged from the effect of mutations in which the node is absent. This leads to a loss of *T* expression in the caudal region of the embryo and severe truncations (Ang and Rossant, 1994; Davidson and Tam, 2000; Weinstein et al., 1994). In this context, there might be an effect of *Oct4* as we observe a clear transition in the behaviour of the *in vitro* populations whether they express *Oct4* (Epi-CE) or not (Epi-NMP). This transition might correspond to the proliferative amplification phase and the start of the differentiation phase of the NMPs. *Oct4* might create a molecular context for *Sox2*; as long both are expressed the cells in the epiblast are multipotent and only when *Oct4* is downregulated, *Sox2* becomes engaged in neural differentiation. It will be interesting to test this hypothesis.

Our study highlights the value of comparing embryonic and *in vitro* derived cell populations. This not only can provide useful information for the derivation of specific populations but might also generate hypothesis and thus provode insights into normal development which might not be obtainable by classical genetic methods.

Materials and Methods

ESC Culture and routine cell culture

E14-Tg2A, Bra::GFP (Fehling et al., 2003), Nodal::YFP (Papanayotou et al., 2014) and Sox17::GFP Ubiquitin::Tomato (Niakan et al., 2010) mouse ESCs were cultured in tissue-culture plastic flasks coated with 0.1% gelatine in PBS (with Calcium and Magnesium), filled with GMEM (Gibco, UK) supplemented with non-essential amino acids, sodium pyruvate, GlutaMAX^{TM}, β-mercaptoethanol, foetal bovine serum and LIF. Cell medium was changed daily and cells passaged every other day.

The differentiation protocols are as the following:

ES-NMP

E14-Tg2A cells were plated at a density of 4.44x10^3 cells/cm^2 in a 0.1% gelatine coated flask with a base medium of N2B27 (NDiff 227, Takara Bio) for 2 days. After 48hr N2B27 is supplemented with 3μM of CHIR99021 (Chiron 10mM, Tocris Biosciences) for additional 24hr, which are in total 72hr.

EpiSCs

E14-Tg2A or Bra:GFP were grown on a 0.5% Plasma Fibronectin (FCOLO, 1mg/ml, Temecula) in PBS (with Calcium and Magnesium) coated culture flask with N2B27 supplemented with 12ng/ml FGF2 (R&D systems, 50μg/ml) and 25ng/ml Activin A (Stem Cells Institute 100μg/ml), known as Epi-media, for at least 4 passages. These cells considered as EpiSCs. Those cells can be tested to be EpiSC by seeding them in a colony assay density (67 cells/cm^2) in restricted medium (2i: N2B27 supplemented with 3μM Chiron and 1μM PD0325901 (PD03, Tocris Biosciences, 10mM)), resulting in no growth of cells, ensuring that the cells are no longer in the naïve pluripotent state and they moved on to the prime pluripotent state (data are not shown).

Epi-CE and Epi-CE-T

EpiSCs were plated at a 5x10^4 cells/cm^2 density in a 0.5% Fibronectin pre-coated flask with Epi-media for the first day. Day 2 is followed by increasing the concentration of FGF2 to 20ng/ml in the base medium of N2B27 and removing Activin A. On day 3, N2B27 is supplemented with 3μM Chiron which is added to the 20ng/ml FGF2. After 72hr those cells known as the Epi-CE. This protocol is a variation of one that has been used to derive NMP-like cells from human ESCs (Lippmann et al., 2015). Epi-CE-T were cultured from Bra:GFP cell line at the same way as Epi-CE with the modification that after 72 hours the cells were sorted for positive GFP cells only.

Epi- NMP

Epi-CE cells were detached from the culture flask using Accutase (BioLegend 0.5Mm) and seeded on a flask coated with 0.5% Fibronectin at a dense of $5x10^4$ cells/cm^2. The cells were grown for 2 days in N2B27 supplemented with 20ng/ml FGF2 and 3μM Chiron.

Single cells transcriptomic

10x Genomics single cell transcriptomic service was used to sequence our 4 different samples. 8,700 cells from each sample were loaded into the 10x Chromium system. The preparation of the libraries and the Illumina sequencing (HiSeq 4000) was done by the Cambridge 10X genomics services. Cell Ranger version 1.3.1 (10x Genomics) was used to process raw sequencing data and the Seurat R package version 2.0 (Butler and Satija, 2017; Macosko et al., 2015) was used to read the data from Cell Ranger to R and build the expression matrix. Gene expression was quantified by UMI counts. The final output was a matrix of genes versus cells, utilized for further analysis.

Embryo data

In this work, we used the published transcriptomic single cell data from 3 mouse embryos females and males at E8.25 (Ibarra-Soria et al., 2018; Pijuan-Sala et al., 2019) including their extra-embryonic tissues. These embryos were dissociated to single cells and processed on a 10X microfluidic chip. The resulting libraries were sequenced on an Illumina HiSeq 2500, subsequent in total 7,006 cells out of which 4,706 are male cells and 2,300 are female cells.

Single cell data clean up and quality control

Using Scater package in R (McCarthy et al., 2017), the expression matrix was cleaned in the 4 following aspects: 1) UMI counts – drawing the histogram of the RNA UMI total counts per cell, allowed us to set a threshold of above 8,000 UMI counts in a cell, ensuring a sufficient sequencing depth for each cell; 2) detected genes – from the histogram of total detected genes in a cell we set a threshold of above 2,500 unique genes in a cell, ensuring the reads are distributed across the transcriptome; 3) mitochondrial genes expression – plotting the per cent of mitochondrial genes counts in a cell versus the total detected genes in a cell, allowed us to set a threshold of 20%, ensuring the cells to be further analyse are not likely to be dead or stressed; 4) Gene filtering – undetectable genes were filtered out by setting a threshold of having at least two cells containing more than 1 UMI of a gene. After the clean up the number of cells and total genes are presented in Table 2.

The UMI count normalization, which is necessary to make accurate comparison of gene expression between samples, was done by first scaling the counts of each gene in a cell to the total counts in that cell per million counts (known as counts per million, CPM). Then the $\log_2$(CPM+1) was calculated for each gene, this is the normalized gene expression (the 1 was added to the CPM to keep zero counts as zero in the binary logarithm scale).

Seurat clustering

We used Seurat, R package version 2.3.4 (Butler et al., 2018; Stuart et al., 2018), for clustering which is based on a community detection approach. This package calculates highly variable genes and focuses on them for downstream analysis. It calculates the average expression and dispersion for each gene, places these genes into bins, and then calculates a z-score for dispersion within each bin. This helps control for the relationship between variability and average expression.

Visualization of the single cell data using SPRING (Weinreb et al., 2017)

SPRING is composed of the following steps:

1. Filters cells with fewer 1000 UMIs.
2. Filters genes with average expression > 0.05 UMIs/cell.
3. Normalize gene expression that every cell has the same total reads.
4. filters for genes with average expression > 0.1 and Fano factor > 3.
5. Z-score normalize expression and reduces dimensionality to a 20 dim PCA space.
6. Compute distance matrix and output k-nearest-neighbour (knn) graph.

This visualization exhibit how cells are positioned in high-dimension with respect to one another.

Clustering the embryo cells

The dissection of CLE in silco from the whole mouse embryo was done by selecting cells that coexpress *Sox2* and *T*; cells that express *Sox2* and *Nkx1-2* and don't express *T* and cells that express *T* and don't express *Sox2*, *Mixl1* and *Bmp4* (see text). Before clustering the embryo CLE cells, a selection of genes was carried out to guide this action. The selection was made to get the focus on the caudal region of the embryo and, importantly, to avoid biases towards clustering results led by genes associated with different processes or regions; for example, the embryo data is a mixture of male and female embryos and in this situation, *Xist* expression leads to clusters of female and males (unpublished observation). The genes that were selected for our analysis were a total of 1,402 genes reported by Koch et al. 2017 in a study of the NMPs and the caudal region of the embryo (Koch et al., 2017). To this list further genes were added due to their association with the CLE region of the E8.5 embryo (Edri et al., 2019), reaching a total of 1,471 genes. From this list, genes with zero mean expression were removed, yielding a total of 1,342 genes for analysis (Table S2). Clustering was performed with the Cell Consensus Clustering (SC3) package in R (Kiselev et al., 2017) with the following steps:.

1. Gene filter – filtering genes that are either expressed in less than *6%* of the cells (rare genes) or expressed in at least 94% of cells (ubiquitous genes).
2. Distance matrices calculations – distances between the cells are calculated using the Euclidean, Pearson and Spearman matrices.
3. Transformations – All distance matrices are then transformed using either principle component analysis or by calculating the eigenvectors of the associated graph Laplacian.
4. k-means – k-means clustering is performed on the first set of eigenvectors of the transformed distance matrices. The number of clusters k is set by the user.
5. Consensus clustering – a binary similarity matrix is constructed for each individual clustering result from the corresponding cell labels obtained in the previous step: if two cells belong to the same cluster, their similarity is 1; otherwise the similarity is 0. A consensus matrix is calculated by averaging all similarity matrices of the individual clustering results. The resulting consensus matrix is clustered using hierarchical clustering.

The clustering of the embryo cells was done between k = 2 and k = 8. The Consensus matrices for the different k are shown in Figure S6. The averaged Silhouette width for each clustering results is summarized in the table below:

The silhouette is a quantitative measure represents the consensus matrix diagonally. An average silhouette width, which is calculated as the weighted average between the silhouette values of each cluster, varies from 0 to 1 and the closest it is to 1 the better the clustering is for that value of k. From the consensus matrices on Figure S6 and from the averaged silhouette width in Table 3, we estimated that the optimal number of clusters could be k = 3 or k = 4. For k = 3, the 3 clusters are: a mixed cluster – containing cells from all the 3 categories: NMP candidates, preNeuro and preMeso; and the two other, mainly composed from preMeso cells (Fig. S6). For k = 4 the clusters are: a mixed cluster composed from all the three cells' categories, 2 others which are mainly composed of cells with a mesodermal

identity and a forth one which is mainly constructed from neural oriented cells (Fig. S6). We decided to continue to downstream analysis with k = 4 because of the appearance of a clear neural along with mesodermal clusters. K = 4 ensures a representation for all the three cells' categories: NMP candidates, mesodermal and neural cells.

Marker genes

Using the SC3 package in R (Kiselev et al., 2017) 96 marker genes were identified for the 4 obtained clusters (see Table S3). Marker genes are defined as genes that are highly expressed in only one of the clusters and can lead to the segregation of one cluster from the rest. Finding the marker genes are according to the following steps as was explained in (Kiselev et al., 2017):

1. Constructing a binary classifier for each gene based on comparing the mean expression values across the clusters.
2. Calculating the classifier prediction by comparing the gene expression ranks across clusters.
3. Quantify the accuracy of the prediction by calculating for each gene the area under the receiver operating characteristic (ROC) curve (true positive rate versus false positive rate).
4. Calculating the p-value for each gene by using the Wilcoxon signed rank test: comparing the gene ranks in the cluster with the highest mean expression with all others.
5. Setting a threshold for the area under the ROC curve and the p-value to determine the marker genes.

The genes with the area under the ROC curve > 0.65 and with the p-value < 0.01 are defined as marker genes. The top 10 marker genes of each cluster are visualized in Fig. 3A.

Mutual information between genes and classes

After identifying the 4 different clusters in the in silico CLE embryo data, the downstream analysis was constructed with the whole set of qualified genes (14,822) rather than with the genes restricted to CLE (1,342). This step was performed to avoid an underrepresentation of genes that were not previously linked to the NMPs. However, there is a need for dimensionality reduction to elucidate the data and to feasibly reduce computer calculation time. Here, similar to the work of Vanitha et al., 2015 (Vanitha et al., 2015), we used a mutual information (MI) technique (Battiti, 1994) to select the informative genes related to the 4 clusters. The steps of computing the MI between the clusters (denoted as Y) and genes (denoted as X) are the following:

1. Calculating the clusters entropy:

$$(1)\ H(Y) = -\sum_{y=1:4} p(y)\log_2\big(p(y)\big)$$

   Where $p(y)$ is the probability of each cluster $y = 1, 2, 3, 4$, which is computed based on the distribution of the 4 clusters in the embryo data.
2. Discretization the gene expression values into ten bins and calculating the conditional entropy $H(Y|X)$ as the following:

$$(2)\ H(Y|X) = \sum_{x} p(x)H(Y|X = x)$$

   Where $p(x)$ is the probability of the discretize expression values of a gene across the cells population and $H(Y|X = x)$ is the clusters entropy given a specific gene expression value, calculated following Equation 1.
3. Computing the MI between the clusters and each gene is accordant the below equation:

$$(3)\ MI(X;Y) = H(Y) - H(Y|X)$$

4. Setting a threshold of the MI of all the genes and selecting the informative genes above this value to train the SVM.

Testing different values of MI between the genes and the clusters in which genes with MI above these values determines which genes are selected as input features for building the SVM (Table 4). The gene selection step helps to remove many irrelevant genes which improves the classification accuracy. As can be seen in Table 4 setting higher threshold to the MI value leads to lower number of informative genes that are fed to the classifier and influence its performance. Using a MI threshold above 0.15, leads to 82 useful genes without damaging the classifier performance.

Multiclass Support vector machine (SVM)

In machine learning SVM is a supervised learning model used either to classification or regression analysis, introduced in 1992 by Boser, Guyon and Vapnik (Boser et al., 1992). Given a labelled training data, an SVM classifies it by finding the best hyperplane that separate all the data points of one class from the other class. The best hyperplane for an SVM means the one with the largest margin between the two classes. The support vectors are the data points that are on the margins of the separating hyperplane. New data points are then mapped into the same space and predicted to belong to a specific class based on which side of the hyperplane they fall. It often happens that the sets to discriminate are not linearly separable in a finite dimensional space. In that case a kernel function is used to map the original finite dimensional space into a much higher dimensional space, making the separation easier in that space. The selection of an appropriate kernel function is important, since it defines the space in which the training set will be classified. Exploring of the different kernel function can be found in our manuscript in preparation, here we show the result of the linear kernel function.

The classification problem in this work is multiclass classification rather than a binary classification. To face this problem, the dominant approach is to reduce the single multiclass problem into multiple binary classification problems. Using the R package e1071 version 1.6.8 (Meyer et al., 2017), the “one-against one” approach was selected in which $n(n-1)/2$ binary classifiers are trained where n is the number of classes (in this work $n = 4$); the appropriate class is assigned by the majority output of a voting scheme.

Choosing SVM in this work as a classifier was due to its high accuracy and its ability to deal with high dimensional data as was proven previously in large scale image classification and gene expression data (Abdullah et al., 2011; Jiang et al., 2007; Lin et al., 2011; Vanitha et al., 2015).

To train the SVM and test the its performance a leave one out cross validation (LOOCV) method was used. In this method, the train data is $N-1$ cells, where N is the total number of cells in the embryo data (*498* cells) and the remaining N^{th} cell is used for testing the model and the same is repeated N times such that each cell is tested, classified and contributing to the model performance (Fig. 3B). The informative genes that passed the MI threshold were used as input features to the SVM. The LOOCV method makes the best use of the available data, especially when the number of samples is small (*498* cells), and avoids the problem of random selection (Ben-Dor et al., 2000).

Predicting the class of the *in vitro* cells

1. Selecting the CLE cells in the same way it was done in the embryo data.
2. Selecting the same informative genes that were used to build the SVM on the embryo data.
3. Inserting the expression matrix of the *in vitro* cells as an input to the SVM.
4. The output is the probabilities of each cell to be assigned to any of the 4 trained clusters.
5. Choosing the dominant class that the cell was assigned in agreement with the maximum probability out of the 4 probabilities (see the plot under Step 6 in Fig. 4A).
6. Since the true classification of the cells is not known and since there might be some hidden classes in the *in vitro* data that were not trained using the embryo data, a harsh constrain needs to be taken: only the cells with minimum probability of 0.8 to be assigned to the dominant class are proceeded to the next step (see the probability plot under Step 6 in Fig. 4A: probability of 0.8 is indicated by the red line).
7. Classification results: only the qualified cells from the previous step are assigned to any of the 4 classes.

Pseudotime analysis

The cells from the *in vitro* samples: ES-NMP, Epi-CE, Epi-CE-T and Epi-NMP, that were classified to the 4 classes (the qualified output cells from the SVM pipeline), went through a pseudotemporal cell ordering. For pseudotime reconstruction of single cell RNA-seq data there are not a lot of available tools that have been systematically tested and have easily accessible software. Moreover, in this work we are analysing a heterogeneous cell population of different conditions rather than cells from a time course experiment, hence the supervised pseudotime reconstruction approaches are not applicable and one should rely on unsupervised methods. We decided to use TSCAN, the Biocounductor R package version 1.16.0, (Ji and Ji, 2017), since it demonstrated reliable unsupervised pseudotime reconstruction results compared to alternative methods (Ji and Ji, 2017).
TSCAN first clusters the cells then it builds a minimum spanning tree to connect the clusters. The branch of this tree that connects the largest number of clusters is the main branch which is used to determine the psedotime order of the cells. This algorithm does not detect starting or ending points and prior biological information is needed to understand the start of the pseudotime order. The pseudotime order might represent the underlying developmental trajectory.

Defining the highly expressed genes in the 2 pseudotime ranges of class 4

1. The cells in class 4 were split to 2 groups based on their pseudotime order: $t_p \leq 1250;\ 2500 \leq t_p \leq 3700$.
2. Identifying the differential expressed genes between the 2 groups using the two sided Wilcoxon rank sum test. The P-value was corrected using the “BY” method of Benjamini and Yekutieli (2001). This method controls the false discovery rate and the proportion of false discoveries amongst the rejected hypotheses.
3. *4,569* differential expressed genes were detected by setting the adjusted $P - value \leq 0.01$.
4. The mean expression of the *4,569* genes across the cells in each group was calculated.
5. Log2 fold between the mean expression of the 2 groups was calculated and the highly expressed genes in each group were defined as the genes that their log2 fold is above 1, resulting in *24* genes in the early pseudotime range and *178* genes in the later range (Table S5).
6. Using the ccRemover R package version 1.0.4 (Barron and Li, 2016) each gene from the identified highly expressed genes could be identified as cycling gene. *55%* of the highly expressed genes in the later pseudotime range group are defined as cycling genes, whereas the cells in the earlier range don’t show this enrichment (no cycling genes).

Statistical test for controlling the sample size

Class 4 is approximately twice the size of class 1, and the node-like cells were assigned almost exclusivity to class 4. Hence, one might think that the different size of the classes might bias the finding of the node-like cells in class 4. The statistical test that was design in this case was aim to control for the size of the classes: randomly 570 cells (half of class1) were selected from class 1 and class 4, and the null hypothesis is that there is no difference in the number of the node-like cells between class 1 and class 4. This step was repeated 1,000 times, resulting that in 1,000 of the cases class 4 contained more node cells than class 1, means that the calculated $p - value < 0.001$ and the null hypothesis was rejected.

Culturing Nodal-YFP cells and ubiquitous-tomato cells

Nodal::YFP and Sox17::GFP Ubiquitin::Tomato cells were cultured under the Epi-CE protocol, we name these cells Epi-CE Nodal and Epi-CE RFP (for red fluorescent protein) respectively. The Epi-CE RFP were further grown to make Epi-NMP (Epi-NMP RFP). After two days of culturing Epi-NMP RFP, we plated a mixture that consists of 50% Epi-NMP RFP positive RFP cells and 50% of positive YFP cells of Epi-CE Nodal, at a total dense of $5x10^4$ cells/cm^2 (Fig. S8A-B). Since after sorting the cells they might be in stress, we decided to culture the mixture for 4 days and not for the normal period of 2 days to let the cells to recover. The mixture was grown in N2B27 supplemented with 20ng/ml FGF2 and 3μM Chiron to make Epi-meso2 (EM2), until sorting the cells to RFP positive (sample named: EM2-RFP+4d, contains only the Ubiquitin::Tomato cells) and RFP negative (sample named: EM2-RFP-4d, contains Nodal::YFP cells and might contain Ubiquitin::Tomato cells that didn't express RFP, see Fig. S8C). This population of cells were compared to the EM2-RFP4d, which are 100% cells of Epi-NMP RFP plated in a flask and cultured for 4 days in N2B27 supplemented with 20ng/ml FGF2 and 3μM Chiron to make Epi-meso2. Total RNA was isolated from the 3 samples: EM2-RFP4d, EM2-RFP+4d and EM2-RFP-4d using Trizol. First strand cDNA synthesis was performed with Superscript III system (Invitrogen) and the quantification of double-stranded DNA obtained with specific genes designed primers, using QuantiFast SYBR Green PCR Master Mix (Qiagen) and the standard cycler program (Qiagen RotorGene Q). The qPCR was done in technical triplicates. The primers that have been used are available in Table 6. Expression values were normalized against the housekeeping gene *Ppia*. Here are the steps to calculate the normalized gene expression values:

1. Identifying the C_t (threshold cycle) for each gene (technical triplicates) and calculating the expression values (2^{-Ct}).
2. Calculating the average and the standard deviation (std) for each gene from the triplicate expression values.
3. Dividing the average and the std of each gene in the expression value of *Ppia*.
4. The gene expression across the different conditions was scaled between 0 to 1.

Cell sorting

Epi-CE Nodal cells were sorted according to their YFP positive fluorescence in a MoFlo sorter (Beckman Coulter) using 488nm laser with emission filter of 530/40 (Fig. S8A) and Epi-NMP RFP cells were sorted according to their RFP positive fluorescence using 647nm laser with emission filter of 610/20 (see Fig. S8B). Cells were collected, counted and replated in N2B27 supplemented with 20ng/ml FGF2 and 3μM Chiron medium to make the mixture of 50% Epi-CE Nodal YFP positive cells with 50% of Epi-NMP RFP positive cells, as it was described above. After 4 days, the mixture was sorted to RFP positive and negative cells in the MoFlo sorter using the same laser and filter sets mentioned above (Fig. S8C).

Acknowledgements
We would like to thank Bertie Gottgens for sharing the embryo data before publication, Meritxell Vinyoles for helping in experimental design and insightful discussion and to James Briscoe, Valerie Wilson and Ben Steventon for insightful discussions.

Funding

This work was supported by Cambridge Trust and Cambridge Philosophical Society scholarships and AJA Karten trust award to S. Edri, a Wellcome Trust Clinical PhD Fellowship (grant numbers 103392/Z/13/Z and 103392/Z/13/A) to W. Jawaid and a Sir Henry Dale Fellowship jointly funded by the Wellcome Trust and BBSRC project grants (No. BB/M023370/1 and BB/P003184/1) to AMA.

Reference

Abdullah, N., Ngah, U. K. and Aziz, S. A. (2011). Image classification of brain MRI using support vector machine. In *2011 IEEE International Conference on Imaging Systems and Techniques*, pp. 242–247. IEEE.

Albors, A. R. and Storey, K. G. (2016). Mapping body-building potential. *Elife* **5**, e14830.

Ang, S.-L. and Rossant, J. (1994). HNF-3β is essential for node and notochord formation in mouse development. *Cell* **78**, 561–574.

Barron, M. and Li, J. (2016). Identifying and removing the cell-cycle effect from single-cell RNA-Sequencing data. *Sci. Rep.* **6**, 33892.

Battiti, R. (1994). Using mutual information for selecting features in supervised neural net learning. *IEEE Trans. Neural Networks* **5**, 537–550.

Beddington, R. S. P. (1982). An autoradio graphic analysis of tissue potency in different regions of the embryonic ectoderm during gastrulation in the mouse. *Embryol. exp. Morph* **69**, 265–285.

Ben-Dor, A., Bruhn, L., Friedman, N., Nachman, I., Schummer, M. and Yakhini, Z. (2000). Tissue Classification with Gene Expression Profiles. *J. Comput. Biol.* **7**, 559–583.

Blum, M., Andre, P., Muders, K., Schweickert, A., Fischer, A., Bitzer, E., Bogusch, S., Beyer, T., van Straaten, H. W. M. and Viebahn, C. (2007). Ciliation and gene expression distinguish between node and posterior notochord in the mammalian embryo. *Differentiation* **75**, 133–146.

Boser, B. E., Guyon, I. M. and Vapnik, V. N. (1992). A training algorithm for optimal margin classifiers. In *Proceedings of the fifth annual workshop on Computational learning theory - COLT '92*, pp. 144–152. New York, New York, USA: ACM Press.

Butler, A. and Satija, R. (2017). Integrated analysis of single cell transcriptomic data across conditions, technologies, and species. *bioRxiv* 164889.

Butler, A., Hoffman, P., Smibert, P., Papalexi, E. and Satija, R. (2018). Integrating single-cell transcriptomic data across different conditions, technologies, and species. *Nat. Biotechnol.* **36**, 411–420.

Cajal, M., Lawson, K. A., Hill, B., Moreau, A., Rao, J., Ross, A., Collignon, J., Camus, A., Simeone, A. and Levi, G. (2012). Clonal and molecular analysis of the prospective anterior neural boundary in the mouse embryo. *Development* **139**, 423–36.

Cambray, N. and Wilson, V. (2007). Two distinct sources for a population of maturing axial progenitors. *Development* **134**, 2829–2840.

Davidson, B. P. and Tam, P. P. (2000). The node of the mouse embryo. *Curr. Biol.* **10**, R617-9.

Downs, K. M. (2008). Systematic localization of Oct-3/4 to the gastrulating mouse conceptus suggests manifold roles in mammalian development. *Dev. Dyn.* **237**, 464–475.

Dunty, W. C., Kennedy, M. W. L., Chalamalasetty, R. B., Campbell, K. and Yamaguchi, T. P. (2014). Transcriptional profiling of Wnt3a mutants identifies Sp transcription factors as essential effectors of the Wnt/β-catenin pathway in neuromesodermal stem cells. *PLoS One* **9**, e87018.

Edri, S., Hayward, P., Baillie-Johnson, P., Steventon, B. and Arias, A. M. (2019). An Epiblast Stem Cell derived multipotent progenitor population for axial extension. *Development* dev.168187.

Fehling, H. J., Lacaud, G., Kubo, A., Kennedy, M., Robertson, S., Keller, G. and Kouskoff, V. (2003). Tracking mesoderm induction and its specification to the hemangioblast during embryonic stem cell differentiation. *Development* **130**, 4217–27.

Funk, M. C., Bera, A. N., Menchen, T., Kuales, G., Thriene, K., Lienkamp, S. S., Dengjel, J., Omran, H., Frank, M. and Arnold, S. J. (2015). Cyclin O (Ccno) functions during deuterosome-mediated centriole amplification of multiciliated cells. *EMBO J.* **34**, 1078–89.

Garriock, R. J., Chalamalasetty, R. B., Kennedy, M. W., Canizales, L. C., Lewandoski, M. and Yamaguchi, T. P. (2015). Lineage tracing of neuromesodermal progenitors reveals novel Wnt-dependent roles in trunk progenitor cell maintenance and differentiation. *Development* **142**, 1628–1638.

Gouti, M., Tsakiridis, A., Wymeersch, F. J., Huang, Y., Kleinjung, J., Wilson, V. and Briscoe, J. (2014). In Vitro Generation of Neuromesodermal Progenitors Reveals Distinct Roles for Wnt Signalling in the Specification of Spinal Cord and Paraxial Mesoderm Identity. *PLoS Biol.* **12**, e1001937.

Gouti, M., Delile, J., Stamataki, D., Wymeersch, F. J., Huang, Y., Kleinjung, J., Wilson, V. and Briscoe, J. (2017). A Gene Regulatory Network Balances Neural and Mesoderm Specification during Vertebrate Trunk Development. *Dev. Cell* **41**, 243–261.e7.

Haghverdi, L., Lun, A. T. L., Morgan, M. D. and Marioni, J. C. (2018). Batch effects in single-cell RNA-sequencing data are corrected by matching mutual nearest neighbors. *Nat. Biotechnol.* **36**, 421–427.

Henrique, D., Abranches, E., Verrier, L. and Storey, K. G. (2015). Neuromesodermal progenitors and the making of the spinal cord. *Development* **142**, 2864–2875.

Huang, S. (2009). Non-genetic heterogeneity of cells in development: more than just noise. *Development* **136**, 3853–62.

Ibarra-Soria, X., Jawaid, W., Pijuan-Sala, B., Ladopoulos, V., Scialdone, A., Jörg, D. J., Tyser, R. C. V., Calero-Nieto, F. J., Mulas, C., Nichols, J., et al. (2018). Defining murine organogenesis at single-cell resolution reveals a role for the leukotriene pathway in regulating blood progenitor formation. *Nat. Cell Biol.* **20**, 127.

Jeong, Y. and Epstein, D. J. (2003a). Distinct regulators of Shh transcription in the floor plate and notochord indicate separate origins for these tissues in the mouse node. *Development* **130**, 3891–902.

Jeong, Y. and Epstein, D. J. (2003b). Distinct regulators of Shh transcription in the floor plate and notochord indicate separate origins for these tissues in the mouse node. *Development* **130**, 3891–902.

Ji, Z. and Ji, H. (2017). TSCAN: Tools for Single-Cell ANalysis.

Jiang, Y., Li, Z., Zhang, L. and Sun, P. (2007). An Improved SVM Classifier for Medical Image Classification. In *Rough Sets and Intelligent Systems Paradigms*, pp. 764–773. Berlin, Heidelberg: Springer Berlin Heidelberg.

Kiselev, V. Y., Kirschner, K., Schaub, M. T., Andrews, T., Yiu, A., Chandra, T., Natarajan, K. N., Reik, W., Barahona, M., Green, A. R., et al. (2017). SC3: consensus clustering of single-cell RNA-seq data. *Nat. Methods* **14**, 483–486.

Koch, F., Scholze, M., Wittler, L., Schifferl, D., Sudheer, S., Grote, P., Timmermann, B., Macura, K. and Herrmann, B. G. (2017). Antagonistic Activities of Sox2 and Brachyury Control the Fate Choice of Neuro-Mesodermal Progenitors. *Dev. Cell* **42**, 514–526.e7.

Kojima, Y., Kaufman-Francis, K., Studdert, J. B., Steiner, K. A., Power, M. D., Loebel, D. A. F., Jones, V., Hor, A., De Alencastro, G., Logan, G. J., et al. (2014). The

transcriptional and functional properties of mouse epiblast stem cells resemble the anterior primitive streak. *Cell Stem Cell* **14**, 107–120.

Lawson, K. A., Dunn, N. R., Roelen, B. A., Zeinstra, L. M., Davis, A. M., Wright, C. V, Korving, J. P. and Hogan, B. L. (1999). Bmp4 is required for the generation of primordial germ cells in the mouse embryo. *Genes Dev.* **13**, 424–36.

Lee, J. D. and Anderson, K. V (2008). Morphogenesis of the node and notochord: the cellular basis for the establishment and maintenance of left-right asymmetry in the mouse. *Dev. Dyn.* **237**, 3464–76.

Lin, Y., Lv, F., Zhu, S., Yang, M., Cour, T., Yu, K., Cao, L. and Huang, T. (2011). Large-scale image classification: Fast feature extraction and SVM training. In *CVPR 2011*, pp. 1689–1696. IEEE.

Lippmann, E. S., Williams, C. E., Ruhl, D. A., Estevez-Silva, M. C., Chapman, E. R., Coon, J. J. and Ashton, R. S. (2015). Deterministic HOX Patterning in Human Pluripotent Stem Cell-Derived Neuroectoderm. *Stem Cell Reports* **4**, 632–644.

Macosko, E. Z., Basu, A., Satija, R., Nemesh, J., Shekhar, K., Goldman, M., Tirosh, I., Bialas, A. R., Kamitaki, N., Martersteck, E. M., et al. (2015). Highly Parallel Genome-wide Expression Profiling of Individual Cells Using Nanoliter Droplets. *Cell* **161**, 1202–1214.

Martinez Arias, A. and Steventon, B. (2018). On the nature and function of organizers. *Development* **145**, dev159525.

McCarthy, D. J., Campbell, K. R., Lun, A. T. L. and Wills, Q. F. (2017). Scater: Pre-processing, quality control, normalization and visualization of single-cell RNA-seq data in R. *Bioinformatics* **33**, 1179–1186.

McGrew, M. J., Sherman, A., Lillico, S. G., Ellard, F. M., Radcliffe, P. A., Gilhooley, H. J., Mitrophanous, K. A., Cambray, N., Wilson, V. and Sang, H. (2008). Localised axial progenitor cell populations in the avian tail bud are not committed to a posterior Hox identity. *Development* **135**, 2289–99.

Meyer, D., Dimitriadou, E., Hornik, K., Weingessel, A. and Leisch, F. (2017). e1071: Misc Functions of the Department of Statistics, Probability Theory Group (Formerly: E1071), TU Wien.

Moris, N., Pina, C. and Arias, A. M. (2016). Transition states and cell fate decisions in epigenetic landscapes. *Nat. Rev. Genet.* **17**, 693–703.

Niakan, K. K., Ji, H., Maehr, R., Vokes, S. A., Rodolfa, K. T., Sherwood, R. I., Yamaki, M., Dimos, J. T., Chen, A. E., Melton, D. A., et al. (2010). Sox17 promotes differentiation in mouse embryonic stem cells by directly regulating extraembryonic gene expression and indirectly antagonizing self-renewal. *Genes Dev.* **24**, 312–26.

Papanayotou, C., Benhaddou, A., Camus, A., Perea-Gomez, A., Jouneau, A., Mezger, V., Langa, F., Ott, S., Sabéran-Djoneidi, D. and Collignon, J. (2014). A Novel Nodal Enhancer Dependent on Pluripotency Factors and Smad2/3 Signaling Conditions a Regulatory Switch During Epiblast Maturation. *PLoS Biol.* **12**, e1001890.

Pijuan-Sala, B., Griffiths, J. A., Guibentif, C., Hiscock, T. W., Jawaid, W., Calero-Nieto, F. J., Mulas, C., Ibarra-Soria, X., Tyser, R. C. V., Ho, D. L. L., et al. (2019). A single-cell molecular map of mouse gastrulation and early organogenesis. *Nature* **566**, 490–495.

Pina, C., Fugazza, C., Tipping, A. J., Brown, J., Soneji, S., Teles, J., Peterson, C. and Enver, T. (2012). Inferring rules of lineage commitment in haematopoiesis. *Nat. Cell Biol.* **14**, 287–94.

Qiu, X., Hill, A., Packer, J., Lin, D., Ma, Y.-A. and Trapnell, C. (2017a). Single-cell mRNA

quantification and differential analysis with Census. *Nat. Methods* **14**, 309–315.

Qiu, X., Mao, Q., Tang, Y., Wang, L., Chawla, R., Pliner, H. A. and Trapnell, C. (2017b). Reversed graph embedding resolves complex single-cell trajectories. *Nat. Methods* **14**, 979–982.

Robb, L., Hartley, L., Begley, C. G., Brodnicki, T. C., Copeland, N. G., Gilbert, D. J., Jenkins, N. A. and Elefanty, A. G. (2000). Cloning, expression analysis, and chromosomal localization of murine and human homologues of aXenopus Mix gene. *Dev. Dyn.* **219**, 497–504.

Schubert, F. R., Fainsod, A., Gruenbaum, Y. and Gruss, P. (1995). Expression of the novel murine homeobox gene Sax-1 in the developing nervous system. *Mech. Dev.* **51**, 99–114.

Selleck, M. A. and Stern, C. D. (1991). Fate mapping and cell lineage analysis of Hensen's node in the chick embryo. *Development* **112**,.

Shiratori, H. and Hamada, H. (2006). The left-right axis in the mouse: from origin to morphology. *Development* **133**, 2095–104.

Steventon, B. and Martinez Arias, A. (2017). Evo-engineering and the cellular and molecular origins of the vertebrate spinal cord. *Dev. Biol.* **432**, 3–13.

Stuart, T., Butler, A., Hoffman, P., Hafemeister, C., Papalexi, E., Mauck, W. M., Stoeckius, M., Smibert, P. and Satija, R. (2018). Comprehensive integration of single cell data. *bioRxiv* 460147.

Tam, P. P. L. and Beddington, R. S. P. (1987). The formation of mesodermal tissues in the mouse embryo during gastrulation and early organogenesis. *Development* **99**, 109–126.

Tam, P. P. . and Behringer, R. R. (1997). Mouse gastrulation: the formation of a mammalian body plan. *Mech. Dev.* **68**, 3–25.

Trapnell, C., Cacchiarelli, D., Grimsby, J., Pokharel, P., Li, S., Morse, M., Lennon, N. J., Livak, K. J., Mikkelsen, T. S. and Rinn, J. L. (2014). The dynamics and regulators of cell fate decisions are revealed by pseudotemporal ordering of single cells. *Nat. Biotechnol.* **32**, 381–386.

Tsakiridis, A. and Wilson, V. (2015). Assessing the bipotency of in vitro-derived neuromesodermal progenitors. *F1000Research* **4**, 100.

Tsakiridis, A., Huang, Y., Blin, G., Skylaki, S., Wymeersch, F., Osorno, R., Economou, C., Karagianni, E., Zhao, S., Lowell, S., et al. (2014). Distinct Wnt-driven primitive streak-like populations reflect in vivo lineage precursors. *Development* **142**, 1209–21.

Turner, D. A., Hayward, P. C., Baillie-Johnson, P., Rué, P., Broome, R., Faunes, F. and Martinez Arias, A. (2014). Wnt/β-catenin and FGF signalling direct the specification and maintenance of a neuromesodermal axial progenitor in ensembles of mouse embryonic stem cells. *Development* **141**, 4243–53.

Vanitha, C. D. A., Devaraj, D. and Venkatesulu, M. (2015). Gene Expression Data Classification Using Support Vector Machine and Mutual Information-based Gene Selection. *Procedia Comput. Sci.* **47**, 13–21.

Weinreb, C., Wolock, S. and Klein, A. M. (2017). SPRING: a kinetic interface for visualizing high dimensional single-cell expression data. *Bioinformatics*.

Weinstein, D. C., Ruiz i Altaba, A., Chen, W. S., Hoodless, P., Prezioso, V. R., Jessell, T. M. and Darnell, J. E. (1994). The winged-helix transcription factor HNF-3β is required for notochord development in the mouse embryo. *Cell* **78**, 575–588.

Wilson, V., Olivera-Martinez, I. and Storey, K. G. (2009). Stem cells, signals and

vertebrate body axis extension. *Development* **136**, 1591–604.

Wolfe, A. D. and Downs, K. M. (2014). Mixl1 localizes to putative axial stem cell reservoirs and their posterior descendants in the mouse embryo. *Gene Expr. Patterns* **15**, 8–20.

Wood, H. B. and Episkopou, V. (1999). Comparative expression of the mouse Sox1, Sox2 and Sox3 genes from pre-gastrulation to early somite stages. *Mech. Dev.* **86**, 197–201.

Wymeersch, F. J., Huang, Y., Blin, G., Cambray, N., Wilkie, R., Wong, F. C. K. and Wilson, V. (2016). Position-dependent plasticity of distinct progenitor types in the primitive streak. *Elife* **5**, e10042.

Wymeersch, F. J., Skylaki, S., Huang, Y., Watson, J. A., Economou, C., Marek-Johnston, C., Tomlinson, S. R. and Wilson, V. (2019). Transcriptionally dynamic progenitor populations organised around a stable niche drive axial patterning. *Development* **146**, dev.168161.

Yamanaka, Y., Tamplin, O. J., Beckers, A., Gossler, A. and Rossant, J. (2007). Live Imaging and Genetic Analysis of Mouse Notochord Formation Reveals Regional Morphogenetic Mechanisms. *Dev. Cell* **13**, 884–896.

Figures

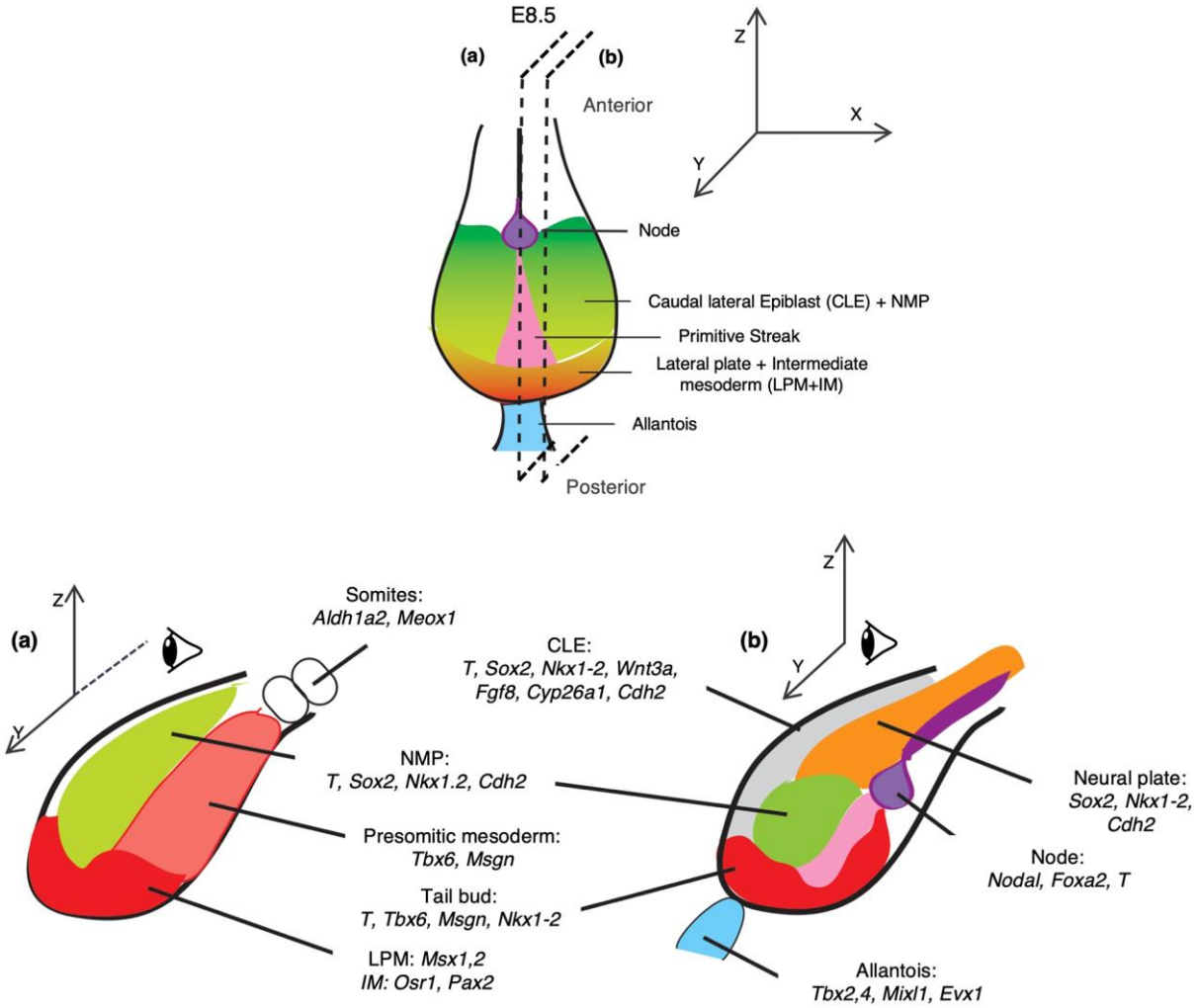

Figure 1. Organization and gene expression patterns in the E8.5 mouse embryo caudal region. Top, ventral view; bottom: lateral (**a**) and medial (**b**) views. The caudal region of the embryo is derived from the posterior epiblast of E7.5 (green in Fig. S1) when the primitive streak (pink) reaches the most distal region of the embryo and the node (purple) appears. This region proliferates and undergoes several morphogenetic events which lead to the organization visible at E8.5 and indicated in the figure. The sources for the outlines shown here can be found in Table S1 and (Edri et al., 2019).

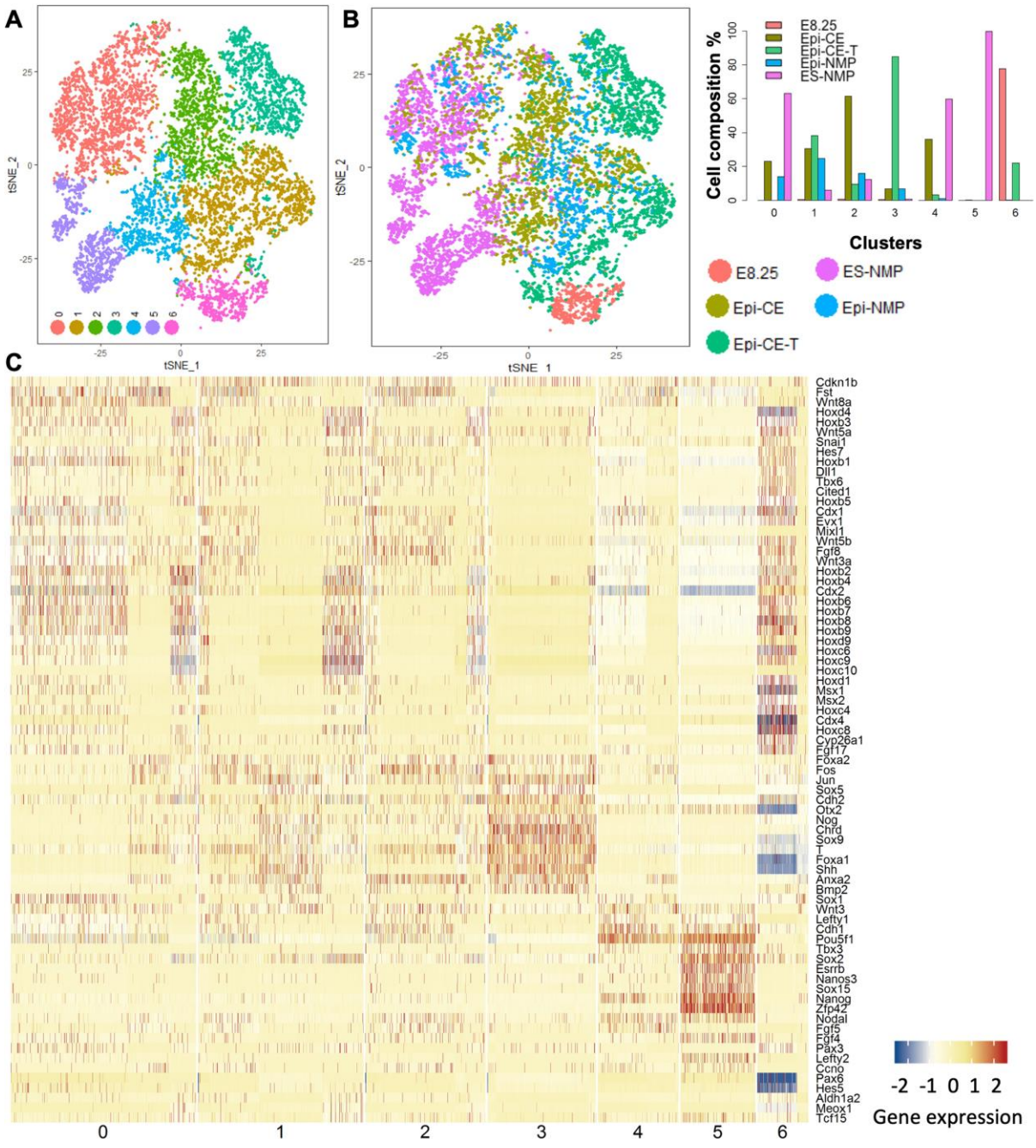

Figure 2. Visualization of the samples and their gene expression along the 7 clusters. **A-B.** tSNE plots coloured by 7 detected clusters (**A**) and the sample names (**B**). **B.** In the right-hand side, the clusters composition of cells from different samples composition can be found. Y-axis represents the percentage of cells from different conditions (colourful bars) in each cluster (x-axis). **C.** Expression of chosen marker genes of pluripotent state, CE (E7.5), CLE, neural, mesoderm and the node along the 7 clusters. The genes are ordered in Hierarchical clustering.

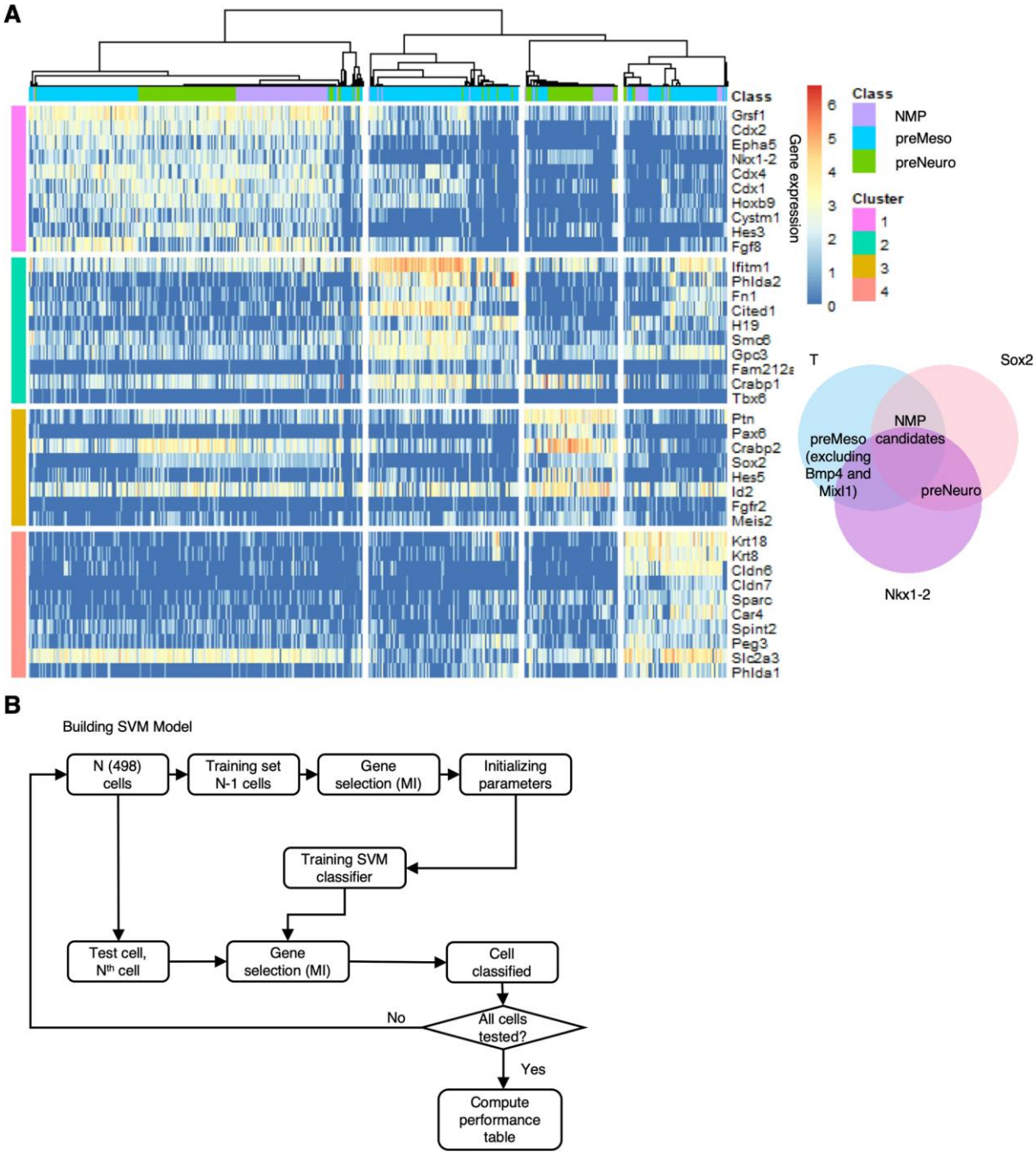

Figure 3. Building SVM based on E8.25 embryo data. A. 498 cells representing the CLE and NSB from three E8.25 embryos were dissected in silico and subjected to an unsupervised clustering approach (SC3 R package (Kiselev et al., 2017), Materials and Methods). This yielded 4 clusters and their marker genes: 1) Pink – genes associated with NMPs; 2) Green – mainly mesodermal genes; 3) Dark yellow – genes associated with neural fate, mainly spinal cord; 4) Peach – genes associated with endoderm, mesoderm and extra embryonic tissue (Table S1). **B.** Leave one out SVM workflow: an iterative process where each cell is trained and tested (Materials and Methods).

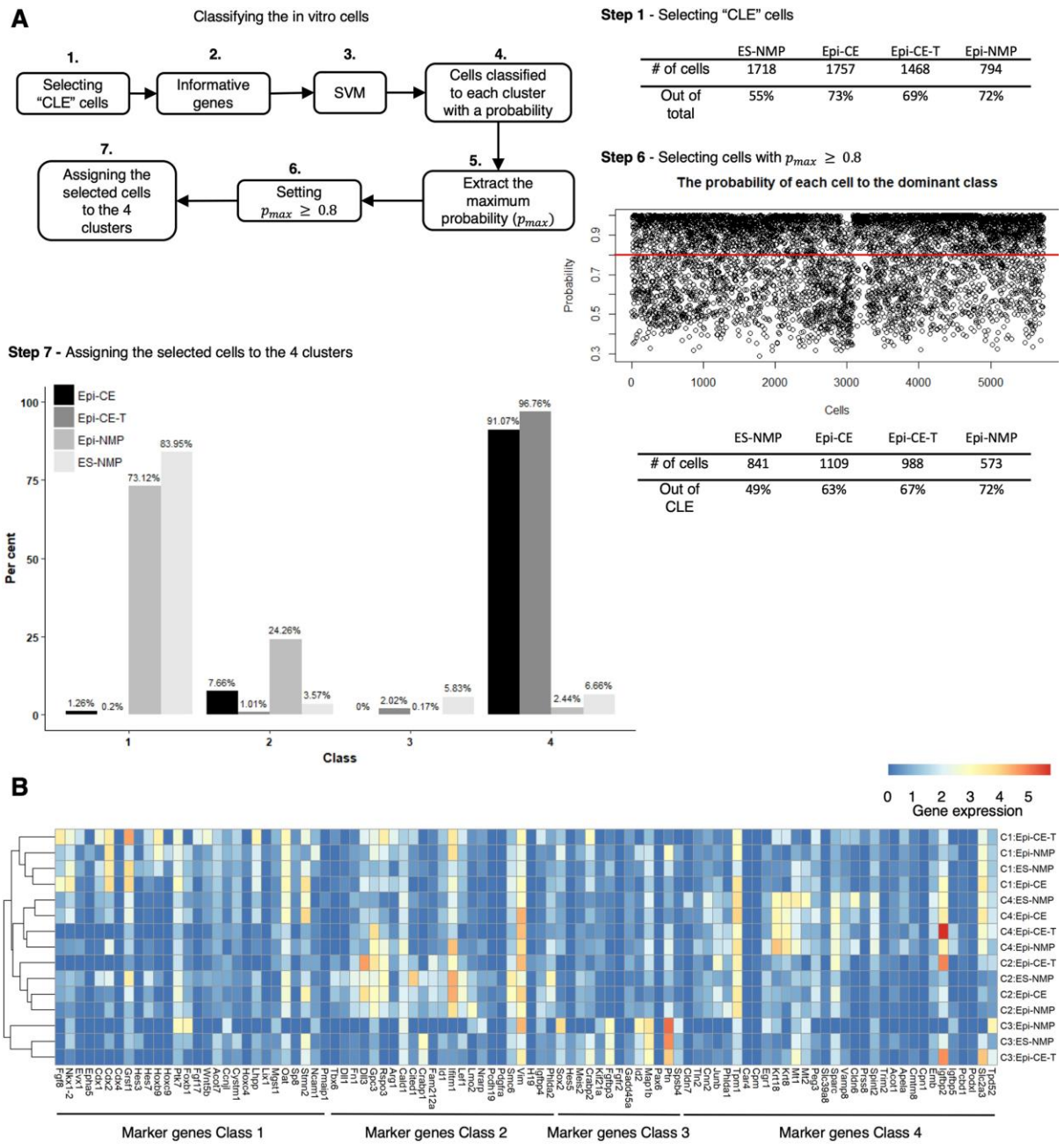

Figure 4. Classifying the *in vitro* cells using the SVM trained on the embryo data A. Workflow of the classification of the *in vitro* cells (for details see text and Materials and Methods). **B.** Average expression of the 96 marker genes found in the embryo of each of the 4 classes, in the *in vitro* samples classified to the 4 classes. Rows of the expression heatmap are hierarchy clustered. Blue-red colour bar indicates the gene expression.

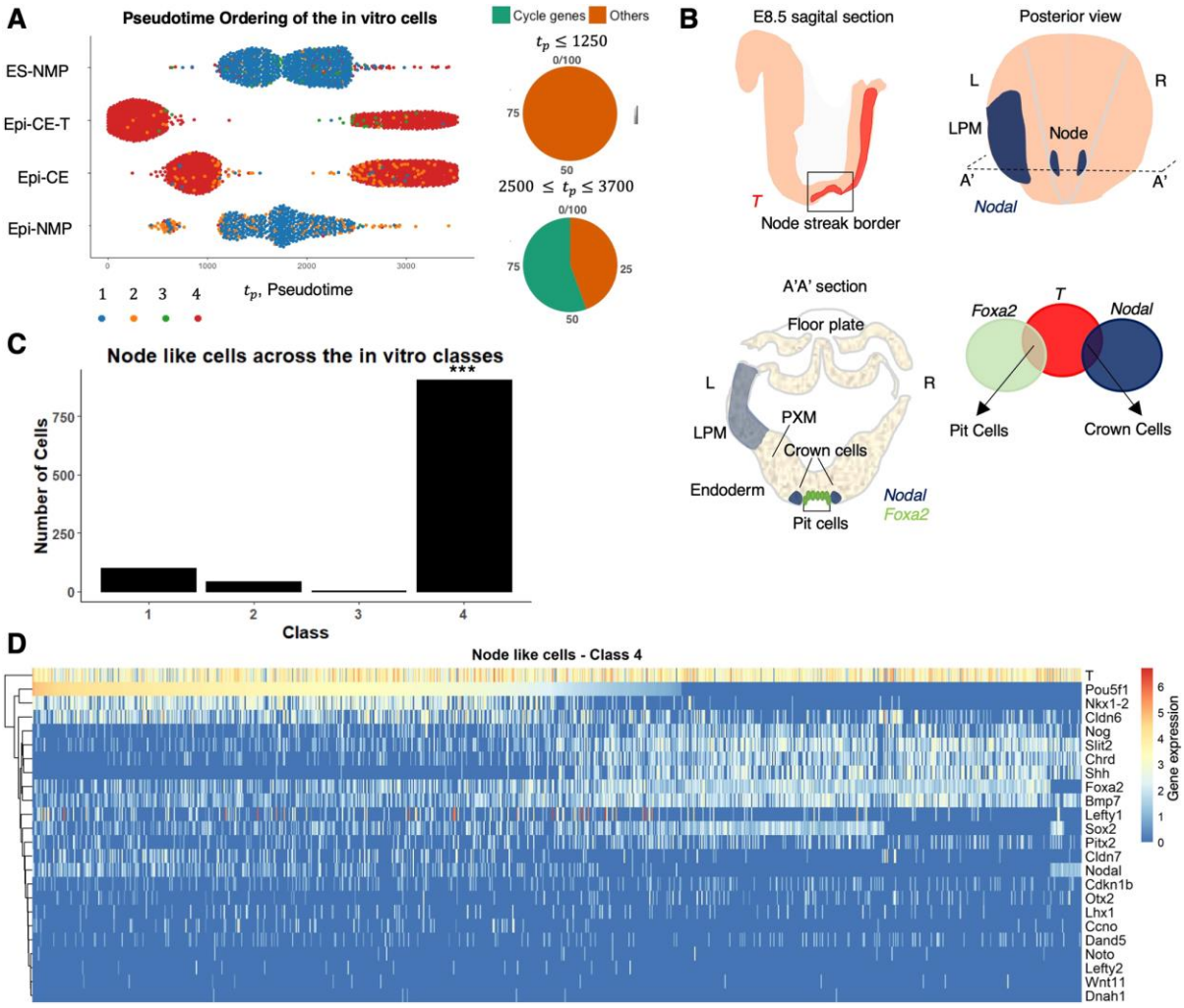

Figure 5. Class 4 contains node-like cells. **A.** Pseudotemporal order of the *in vitro* cells that were classified to the 4 classes. Class 4 is divided to 2 pseudotime ranges: the highly expressed genes in the later range contains 55% of cycling genes whereas the early one doesn't contain any cycling genes (Materials and Methods). **B**. E8.5 mouse embryo node: illustration of a sagittal view of the embryo shows the expression of *T* (red) in the NSB (Tsakiridis et al., 2014). Posterior view of the embryo exhibits the expression of *Nodal* (blue) in the node and in the LPM (Shiratori and Hamada, 2006) and its left (L) right (R) asymmetry. A transverse section (A'A') reveals the pit and crown cells of the node, PXM, LPM, endoderm and the prospective floor plate. The expression of *Nodal* and *Foxa2* is indicated in blue and green respectively. The pit cells coexpress *T* and *Foxa2* and the crown cells express *Nodal* and *T* (Davidson and Tam, 2000; Jeong and Epstein, 2003a; Lee and Anderson, 2008; Shiratori and Hamada, 2006). **C.** The distribution of the node-like cells amongst the 4 classes: significant higher number of the node-like cells are found in class 4 in comparison to the other classes. **D.** Gene expression heatmap of chosen node genes in class 4. The genes are hierarchically clustered and the cells are ordered in accordance with the decreasing expression of *Oct4* (*Pou5f1)*. Gene expression, which is defined as $log_2(CPM + 1)$ (Materials and Methods), is indicated by the blue-red colour bar.

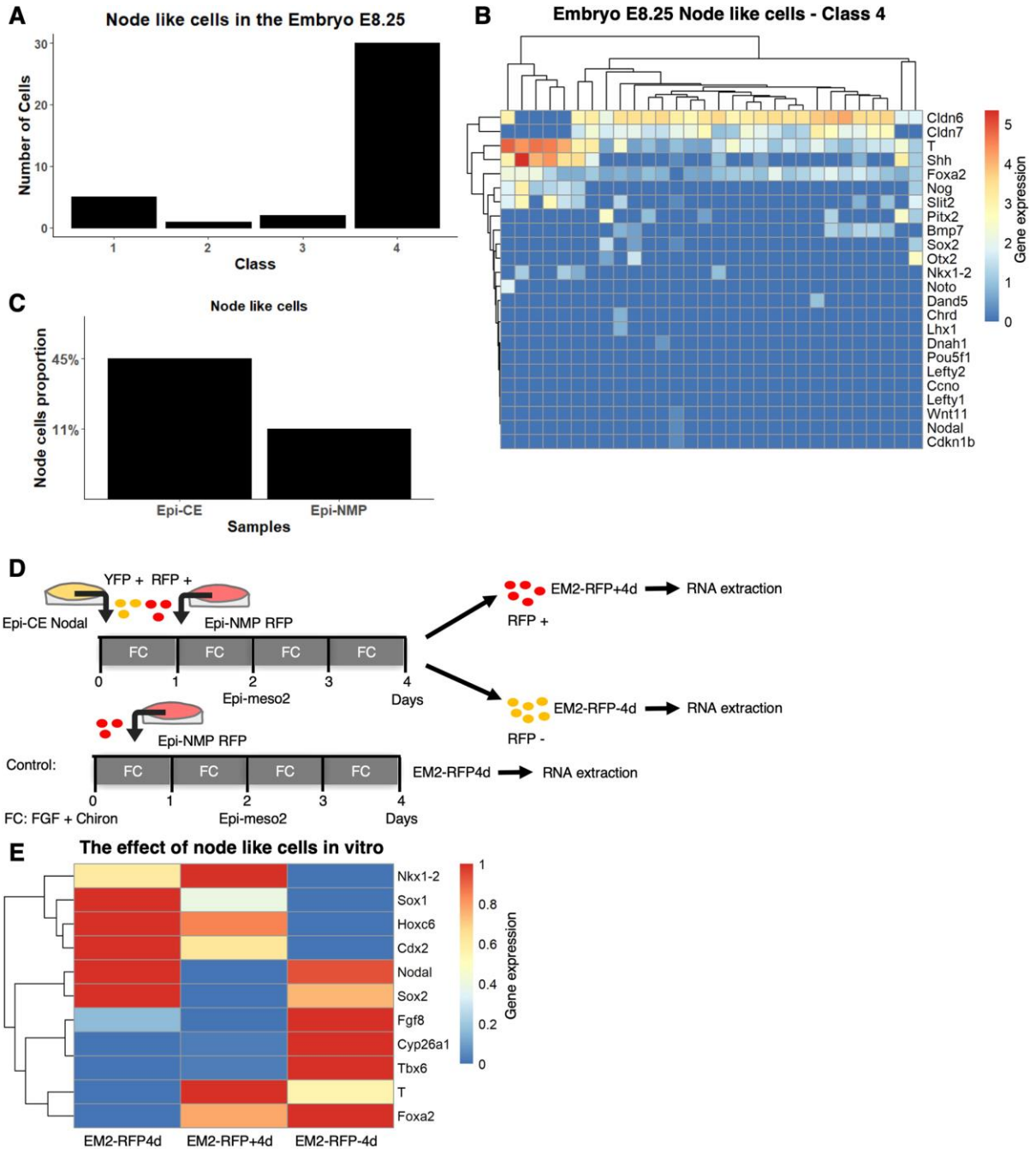

Figure 6. Node cells are needed to maintain the NMPs. A. The distribution of the node cells amongst the 4 classes in the embryo. **B.** Expression of chosen node genes in the embryo class 4. Genes and cells are hierarchically clustered. Gene expression which is defined as $log_2(CPM + 1)$, is indicated by the blue-red colour bar. **C.** Proportion of node-like cells in the Epi-CE and Epi-NMP samples. **D.** YFP positive cells of Epi-CE Nodal sample composed of Nodal::YFP cells and RFP positive cells of Epi-NMP RFP sample composed of Ubiquitin::Tomato cells, were used to make Epi-meso2 mixture (Materials and Methods). This mixture was grown for 4 days then the cells were sorted based on their RFP fluorescence: RFP positive cells (sample named EM2-RFP+4d) and RFP negative cells (sample named EM2-RFP-4d). the control sample is Epi-NMP RFP sample composed of 100% Ubiquitin::Tomato cells that was cultured for 4 days in FGF and Chiron to make Epi-meso2 (sample named EM2-RFP4d). The sorted cells and the control sample were quantified for their mRNA of a chosen set of genes using RT-qPCR technique. **E.** Expression heatmap of 11 genes, obtained by RT-qPCR, in cells grown in the 3 conditions, as indicated in Fig. 6D. The normalized expression of each gene to the housekeeping gene *Ppia* was scaled between 0 and 1 across the different conditions. Gene expression is indicated by the blue-red colour bar.

Table 1 –
The distribution of the node-like cells in the 2 pseudotime ranges of class 4 of the *in vitro* cells.

	Pseudotime range	Class 4	Node-like cells	Out of class 4
Time group 1	$tp \leq 1250$	1050	433	41%
Time group 2	$2500 \leq tp \leq 3700$	916	442	48%

Sample	Total cells	Total genes
ES-NMP	3,133	14,822
Epi-CE	2,404	14,822
Epi-CE-T	2,135	14,822
Epi-NMP	1,108	14,822
Embryo E8.25	4,183	14,822

Table 2. The number of cells in each sample and the total number of detected genes after single cell data clean up.

	k = 2	k = 3	k = 4	k = 5	k = 6	k = 7	k =8
Averaged Silhouette width	0.8	0.9	0.85	0.78	0.77	0.77	0.72

Table 3. The averaged Silhouette width of the consensus matrices obtained for clusters ranging from k = 2 to k = 8.

	Number of informative genes	Correctly classified	Misclassified	Error rate
MI > 0.05	455	483	15	3%
MI > 0.1	158	482	16	3%
MI > 0.15	82	483	15	3%

MI > 0.2	51	477	21	4%
MI > 0.3	17	464	34	7%

Table 4 – Performance of the SVM with setting different threshold of the MI value

	Class 1	**Class 2**	**Class 3**	**Class 4**
Number of cells	1141	264	70	2036

Table 5. The number of the *in vitro* cells classified to the 4 clusters.

	Gene	**Forward Primer Sequence**	**Reverse Primer Sequence**
1	*Cdx2*	TCCTGCTGACTGCTTTCTGA	CCCTTCCTGATTTGTGGAGA
2	*Cyp26a1*	TCTGGGACCTGTACTGTGTGA	AAGCCGTATTTCCTGCGCTT
3	*Fgf8*	AGGACTGCGTATTCACAGAGAT	CATGTACCAGCCCTCGTACT
4	*Foxa2*	CATTACGCCTTCAACCACCC	GGTAGTGCATGACCTGTTCG
5	*Hoxc6*	CCCTCTCTTCTCCCTTGCTC	CCACGTCTGACTCCCTGTTT
6	*Nkx1-2*	ACAACCACACAAGCCACTGA	CCATCCTGGGAACCCTTATT
7	*Nodal*	AGCCACTGTCCAGTTCTCCAG	GTGTCTGCCAAGCATACATCTC
8	*Sox1*	AGACAGCGTGCCTTTGATTT	TGGGATAAGACCTGGGTGAG
9	*Sox2*	CATGAGAGCAAGTACTGGCAAG	CCAACGATATCAACCTGCATGG
10	*T*	CTGGGAGCTCAGTTCTTTCG	GTCCACGAGGCTATGAGGAG
11	*Tbx6*	CCAGAACCCTAGGATCACACA	CCCGAAGTTTCCTCTTCACA

Table 6. Primer sequences used for qRT-PCR.

Table S1 - Genes expression in the mouse embryo

genes	Expression in the embryo E7.5 or E8.5	Category or pattern of expression	References
Nanog	-	Pluripotency and germ cells	(Chambers et al., 2003; Chambers et al., 2007)
Rex1	-	Pluripotency	(Toyooka et al., 2008)
Esrrb	-	Pluripotency	(Festuccia et al., 2012; Papp and Plath, 2012)
Fgf4	CE E7.5 and some expression in the CLE E8.5/9: the expression moves from the primitive streak to a region of the dorsal CE	Pluripotency and expression in the streak	(Niswander and Martin, 1992; Wright et al., 2003)
Sox15	-	Pluripotency	(Maruyama et al., 2005)
Nanos	-	Germ cells	(Tsuda et al., 2003)
Tbx3	-	Pluripotency and germ cells	(Pontecorvi et al., 2008; Russell et al., 2015)
Anxa2		Early epiblast	(Wang et al., 2015)
Fgf5	CE E7.5	Early epiblast	(Hebert et al., 1991; Khoa et al., 2016)
Otx2	CE E7.5	Early epiblast, primitive streak and node	(Acampora et al., 2009; Cajal et al., 2012)
Cdh1	CE E7.5	Pluripotency and early epiblast	(Basilicata et al., 2016; Cano et al., 2000; De Vries et al., 2004; Redmer et al., 2011)
Oct4 (Pou5f1)	CE E7.5	Pluripotency, early epiblast, caudal epiblast until E8.0	(Downs, 2008; Shi and Jin, 2010)
Pou3f1	Expression from E5.5 onward.	Early expression in the anterior epiblast, later expression in the nervous system (midbrain and forebrain) and in the peripheral nervous system. At	(Zhu et al., 2014)

		E8.0 Pouu3f1 expression is restricted to the anterior neuroectoderm.	
Pou4f1	E9.5	Cardiac development and development of cochleovestibular ganglion neurons in mouse inner ear.	(Deng et al., 2014; Maskell et al., 2017)
Tcf15	-	Pre gastrulation, primed pluripotency and somites.	(Davies et al., 2013)
Cdh2	CLE E8.5/9	Primitive streak and neural progenitors	(Basilicata et al., 2016)
Cdx1, Cdx2, Cdx4	Both in CE E7.5 and CLE E8.5/9	Caudal epiblast and tail but (also posterior endoderm)	(Deschamps and van Nes, 2005)
Sox2	Both in CE E7.5 and CLE E8.5/9	Pluripotency, neural progenitors	(Henrique et al., 2015)
T	Both in CE E7.5 and CLE E8.5/9	Primitive Streak, caudal epiblast, tail bud and node.	(Henrique et al., 2015)
Cyp26a1	CLE E8.5/9	Caudal epiblast and tail bud from E8.0	(Sakai et al., 2001; Sirbu and Duester, 2006)
Nkx1-2	Both in CE E7.5 and CLE E8.5/9	Caudal epiblast and tail bud from E8.0; preneural spinal cord	(Henrique et al., 2015; Schubert et al., 1995)
Fgf8	Both in CE E7.5 and CLE E8.5/9	Caudal epiblast and tail bud	(Cunningham et al., 2015; Dunty et al., 2008; Sirbu and Duester, 2006)
Epha5	CLE E8.5/9	At E9.0 expression in the tail bud.	(Cooper et al., 2009)
Fos, Jun		Not known	
Fst1	CE E7.5	It is turned off in the CLE with the onset of somitogenesis.	(Cunningham et al., 2016)
Tbx6	Starts at CE E7.5	Paraxial mesoderm	(Chalamalasetty et al., 2011; Chalamalasetty et al., 2014; Dunty et

			al., 2008; White et al., 2003)
Meox1	CLE E8.5/9	Presomitic and somatic mesoderm	(Jukkola et al., 2005)
Aldh1a2	Both in CE E7.5 and CLE E8.5/9	Paraxial mesoderm at E7.5, presomitic and somatic mesoderm.	(Duester, 2008; Sirbu and Duester, 2006)
Cited1	CLE E8.5/9	Mesoderm. Early kidney development, progenitors of the heart, limb, axial skeleton and placenta.	(Boyle et al., 2007; Dunwoodie et al., 1998; Rodriguez et al., 2004)
Mesp1	From gastrulation E6.5 onwards.	Initially Mesp1 was expressed at the onset of gastrulation in the primitive streak and then in cardiac mesoderm. At E7.5 expression in the base of the allantois. At E8.0 Mesp1 is expressed on both sides of the node.	(Saga et al., 1996; Saga et al., 1997)
Mesp2	Initially detected at E8.0	At E8.0 expression was detected on both sides of the node at the same locations as for Mesp1. From E8.5 expressed in the PSM until E12.5.	(Saga et al., 1997)
Ifitm1	CLE E8.5/9	At E7.5 expression in the allantois. At E8.5 expression in the brain and in the neural tube. At E9.5 expression in the brain, primordial gut, the somites and the PSM. Expression in primordial germ cells (PGCs).	(Klymiuk et al., 2012; Lange et al., 2003)

Fn1		At E10 fibronectin matrix enriched at intersomitic borders.	(Bajanca et al., 2004)
Snai1	CE E7.5	EMT.	(Carver et al., 2001)
Bmp2	Both in CE E7.5 and CLE E8.5/9	IM, extra embryonic tissue (yolk sac and allantois), at E8.25 expression in the neural fold and LPM.	(Danesh et al., 2009)
Bmp4	Both in CE E7.5 and CLE E8.5/9	embryonic tissue (yolk sac and allantois), posterior part of the embryo, at E8.25 high expression in the posterior LPM, neural tube and in the caudal mesoderm of the tail.	(Danesh et al., 2009; Lawson et al., 1999; Zakin and De Robertis, 2004)
Evx1	Both in CE E7.5 and CLE E8.5/9	Posterior primitive streak. At E8.5 expression in the tail bud and in the allantois.	(Cambray and Wilson, 2007; Kojima et al., 2014; Schubert et al., 1995)
Mixl1	CE E7.5 and E8.5/9	Primitive streak, progenitors of endoderm. At E8.5 some expression in the tip of the tail bud and in the allantois, also expression in the crown cells of the node.	(Dunty et al., 2014; Hart et al., 2002; Kojima et al., 2014; Pearce and Evans, 1999; Robb et al., 2000; Wolfe and Downs, 2014)
Foxb1	E8.5	At E8.5 expression in the somites, presomitic mesoderm and in the neural plate	(Zhao et al., 2007).
Fgf3	Both in CE E7.5 and CLE E8.5/9	Fgf3 together with Fgf8 and Fgf17 are expressed in the in the primitive streak, PSM and tail bud. Later (E9.5) expressed in the ectoderm	(Bachler and Neubüser, 2001; Wahl et al., 2007)

		covering the midfacial region.	
Fgf9	Detected from E9.5.	At E9.5 together with Fgf3, Fgf8 and Fgf17, is expressed in the ectoderm covering the midfacial region. At E10.5 expressed the epithelium of the developing lung.	(Bachler and Neubüser, 2001; del Moral et al., 2006)
Fgf15	Expression detected at E9.5	Expressed in the developing CNS	(Fischer et al., 2011)
Fgf17	Low expression in the primitive streak at E7.5 and in the CLE E8.5	expressed in prestreak- and streak-stage embryos. Lower expression than Fgf8 in the posterior primitive streak and then in the presumptive mid/hindbrain junction, presomitic mesoderm and developing heart.	(Maruoka et al., 1998; Sun et al., 1999)
Msx1, Msx2	Starts at E7.5	At E7.5 expression in the embryonic and extraembryonic mesoderm (including the allantois), at E8.0 expression in the LPM and in the visceral endoderm together with the primordial germ cells, expression in the neural crest.	(Ishii et al., 2005; Sun et al., 2016)
Osr1	E8.5	At E8.5 expression in IM. Later expression in the developing heart, limb, lung, and craniofacial structures.	(Lan et al., 2011; Wang et al., 2005)
Phlda2	E8.0-8.5	yolk sac endoderm (expression in the	(Hou et al., 2007; Lefebvre, 2012)

		placenta), LPM and ventral definitive endoderm	
Krt18, Kr8		Extra embryonic endoderm	(Maurer et al., 2008)
Cldn6, Cldn7	At E6.5-E7.5 Cldn6 expressed in the epiblast excluding the primitive streak. At E8.5 expression begins to be restricted to the endoderm.	Definitive endoderm, kidney development	(Anderson et al., 2008; Khairallah et al., 2014)
Sparc	E9.0	At E9.0 present in extra embryonic tissues, later expressed in the parietal endoderm.	(Howe et al., 1988)
Pax6	E8.0 in the neuroepithelium	Spinal cord	(Bel-Vialar et al., 2007)
Pax3	First detected at E8.5	Expressed in the developing spinal cord, later (10-12 day) in the neural crest. Also, marker of limb muscle progenitor cells and expression in the dorsal neural tube.	(Goulding et al., 1991; Relaix et al., 2004)
Sox1	Detected at E7.5 and continue to be expressed at E9.5	Spinal cord: neural plate and neural tube	(Pevny et al., 1998; Wood and Episkopou, 1999)
Sox3	Sox2 and Sox3 expressed early in the embryo at E6.5 and at E8.5.	Both Sox2 and Sox3 are expressed throughout the epiblast. At E7.5 Sox3 is expressed in the posterior epiblast. At E8.5 Sox3 shows anteroposterior gradients of expression with bias to the posterior region.	(Wood and Episkopou, 1999)
Sox9	Expression starts at E9.5	Involved in chondrogenesis, formation of	(Barrionuevo et al., 2006; Wright et al., 1995)

		cardiac valves, and neural crest, testis and spinal cord development. Also expressed in the notochord.	
Sox5	Later expression than E9.0	Involved together with Sox6 in chondrogenesis.	(Akiyama et al., 2002)
Sox6	Later expression than E9.0	Expressed in wide range of tissues amongst them: the central nervous system (brain and spinal cord), somites, notochord, limb buds and liver.	(Akiyama et al., 2002; Hagiwara, 2011)
Sema3a	Expression detected at E9.5	Expression in the peripheral nervous system (PNS) and in the somites.	(Fujisawa and Kitsukawa, 1998; Schwarz et al., 2009)
Hes3	Both in CE E7.5 and CLE E8.5/9	At E7.5 expressed in the primitive streak, at E8.5 expression in the hindbrain, the neural plate and primitive streak.	(Lobe, 1997)
Hes5	First detected at E8-8.5	Neuroepithelium: midbrain, hindbrain and neural tube.	(Hitoshi et al., 2011)
Hes7	CLE E8.5	Expression in the PSM.	(Bessho et al., 2001a; Bessho et al., 2001b)
Ptn		Expressed in the central and peripheral nervous system	(Rosenfield et al., 2012)
Crabp2		At E10.5 can be detected in the spinal cord.	(Colbert et al., 1995; Duester, 2008)
Wnt3	First expressed at E5.5 and at E7.5 expression is evident in the epiblast.	Expression in the posterior visceral endoderm (E5.5) and later in the adjacent posterior epiblast.	(Tortelote et al., 2013)(Stuckey et al., 2011)
Wnt3a, Wnt8a	Both in CE E7.5 and CLE E8.5/9	Caudal epiblast and tail bud.	(Cambray and Wilson, 2007; Cunningham et al., 2015; Girós et al.,

			2011; Parr Brian A. et al., 1993)
Wnt5a	CLE E8.5/9	Caudal epiblast and tail bud.	(Yamaguchi et al., 1999)
Nodal	CE E7.5	Expression in the node.	(Lu and Robertson, 2004)
Foxa2	CE E7.5	Marker of the node and anterior mesendoderm. Also expressed in the extraembryonic tissue.	(Kojima et al., 2014; Lu and Robertson, 2004)
Ccno	CE E7.5-E8.0	Expression in the node and in the posterior tip of the embryo.	(Funk et al., 2015)
Zic1, Zic2, Zic3	From E8.0 to E16.5. Expressed in the CLE.	Expression in the CNS, somites, limb (not Zic1) and eye. Around E8.0, all the three expressed in the dorsal spinal cord and in the somites, Zic1 is evenly distributed along the AP axis but no expression was detected in the tail bud. Zic2 and Zic3 are highly expressed in the head and in the tail bud, but weekly in the trunk.	(Nagai et al., 1997)
Hox5-10	CLE E8.5 – E10.5	Anterior – posterior patterning, specify segment identity. Expression from the last cervical vertebrae (ribs) till the first sacral vertebrae (pelvis).	(Myers, 2008)
Hoxc10	Expression at E10.5		(Lee et al., 1999)

Table S2 – List of genes that were used to cluster the embryo cells (attached xls file).

Click here to Download Table S2

Table S3 – The marker genes of the 4 clusters of the CLE embryo data (attached xls file).

Click here to Download Table S3

Table S4 – The *82* informative genes that were used to build the SVM and classify the cells to the 4 clusters

Click here to Download Table S4

Table S5 – The highly expressed genes in the 2 pseudotime ranges of class 4 (attached xls file).

Click here to Download Table S5

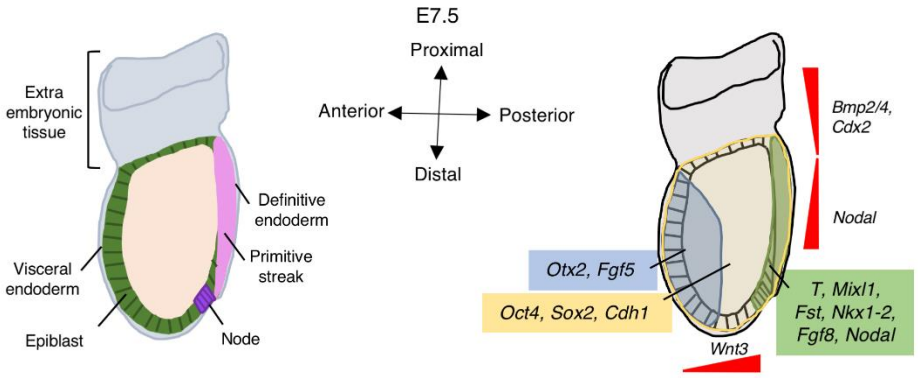

Figure S1. Organization and gene expression patterns in the mouse embryo at E7.5. Lateral view of the mouse embryo at E7.5 with the anterior side to the left. The illustration on the left-hand side indicates the different tissue layers and structures of the embryo, and the one to the right depicts the main gene expression pattern in those regions. The sources for the outlines shown here can be found in Table S1 and (Edri et al., 2018).

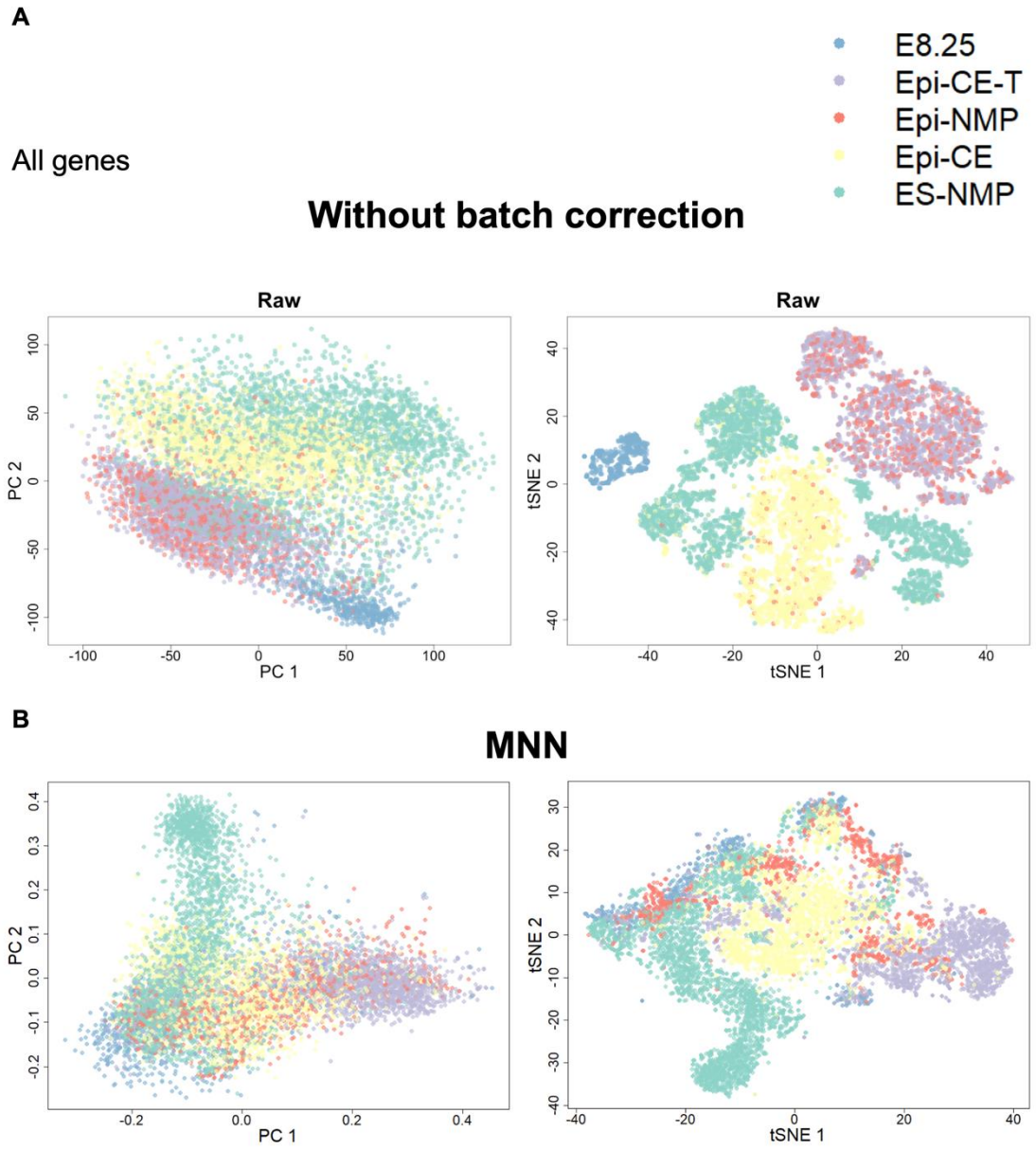

Figure S2. Correction for RNA-seq single cells technical variation. A. PCA and tSNE plots of the raw data after completing the quality control for the cells and genes. The plots were performed using all genes (14,822 genes) that passed the quality control. **B.** Batch effects correction using mutual nearest neighbour (MNN, (Haghverdi et al., 2018)).

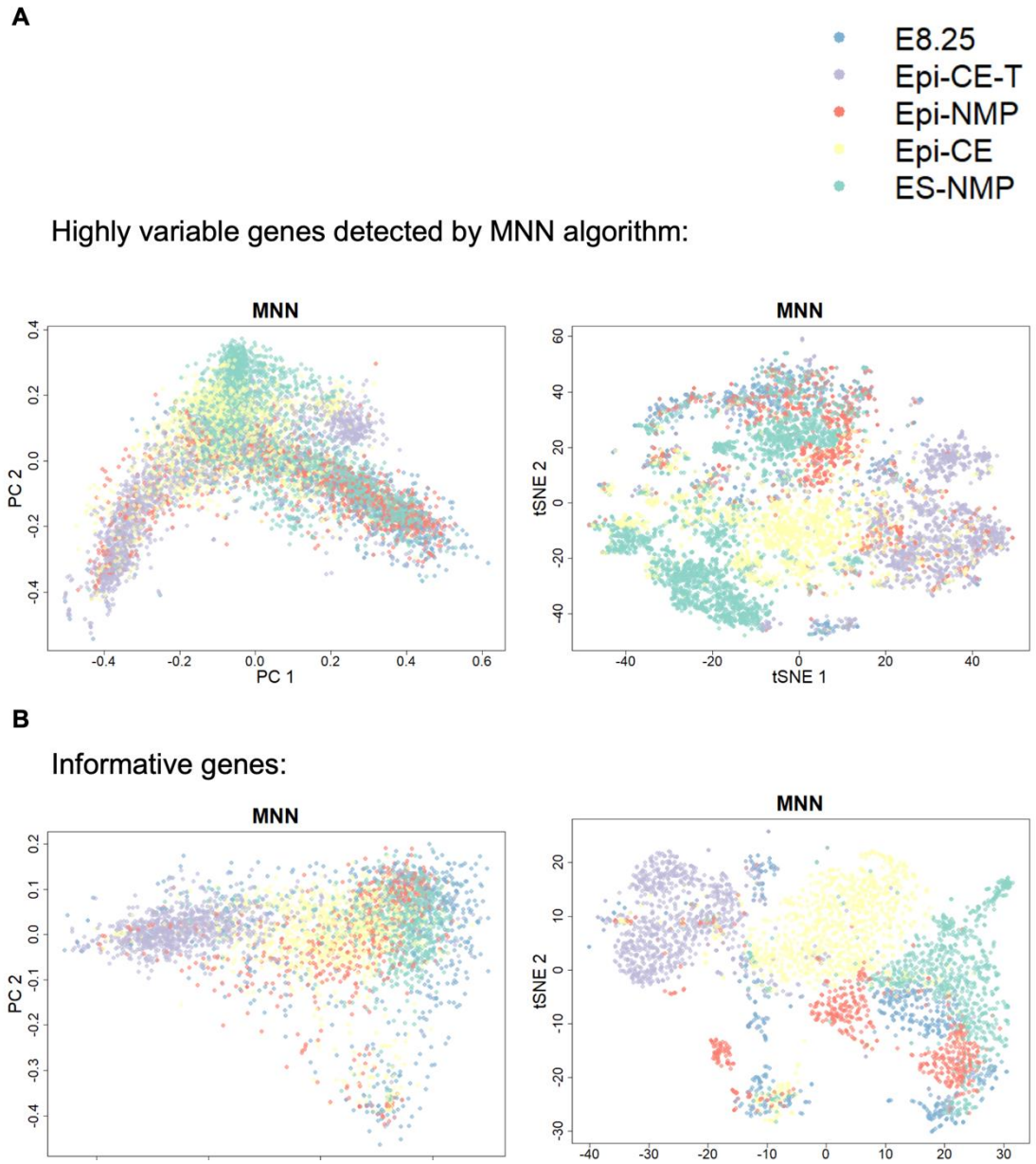

Figure S3. Correction for RNA-seq single cells technical variation for subset of genes. A. MNN batch effects correction using the highly variable genes detected by MNN. **B.** MNN batch effects correction using 1,342 genes of interest gathered from a literature review (see main text and Table S2).

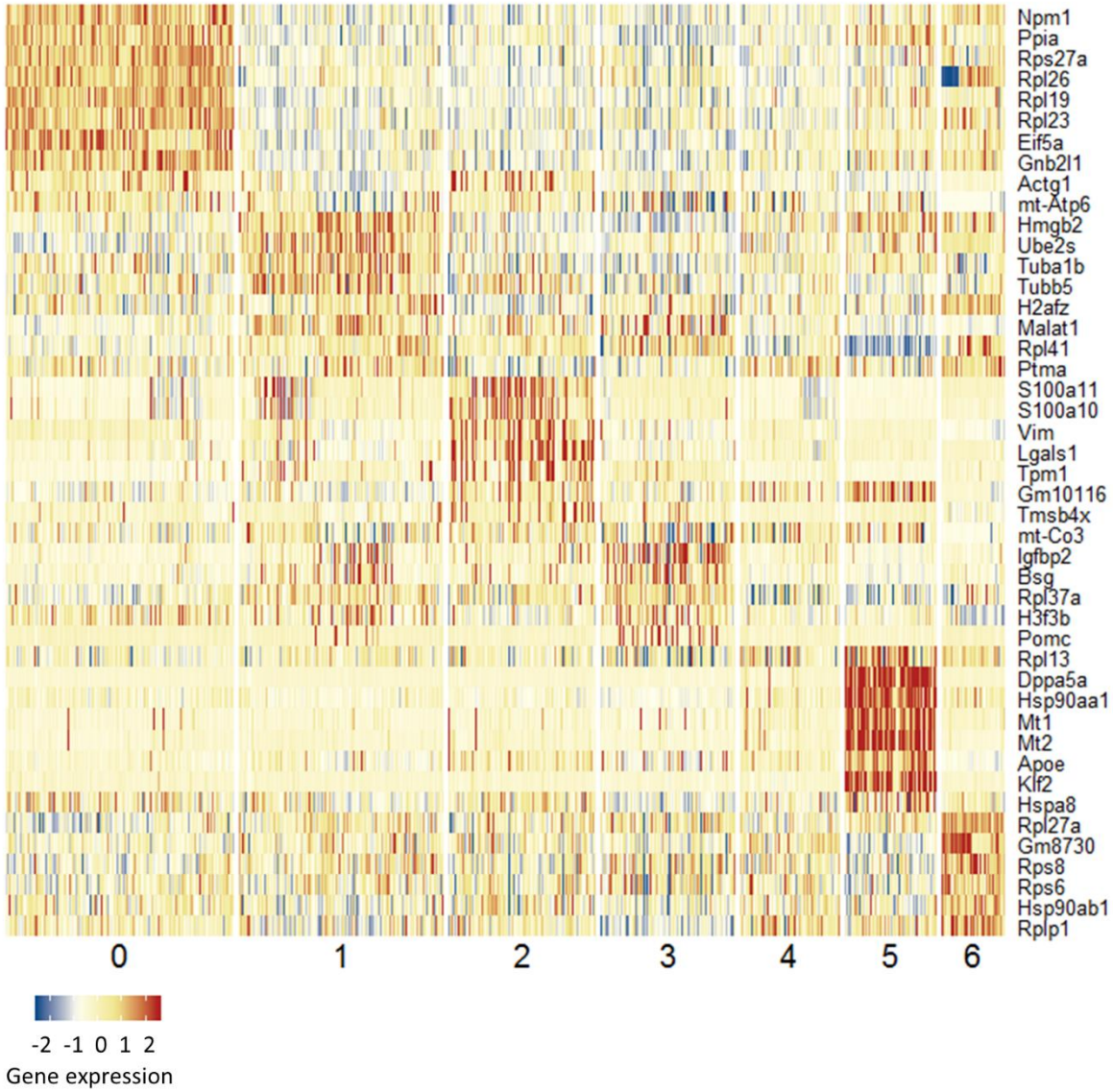

Figure S4. Clustering the embryo dataset and the *in vitro* populations after batch correcting process. Top 10 marker genes characterizing each of the 7 clusters obtained by Seurat package.

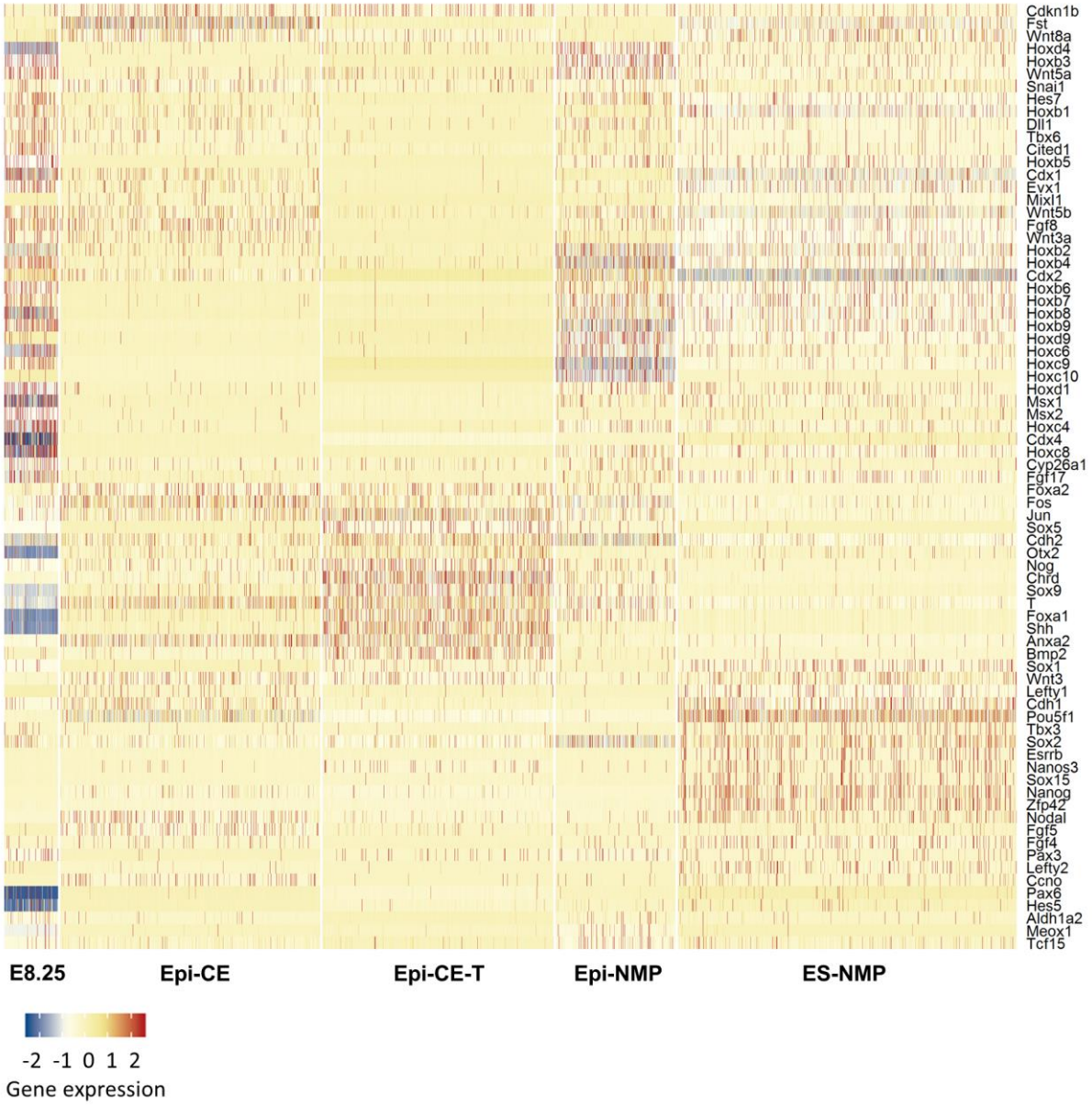

Figure S5. Visualization of gene expression in the *in vivo* and *in vitro* populations. Expression of chosen marker genes of pluripotent state, CE (E7.5), CLE, neural, mesoderm and the node along the different samples.

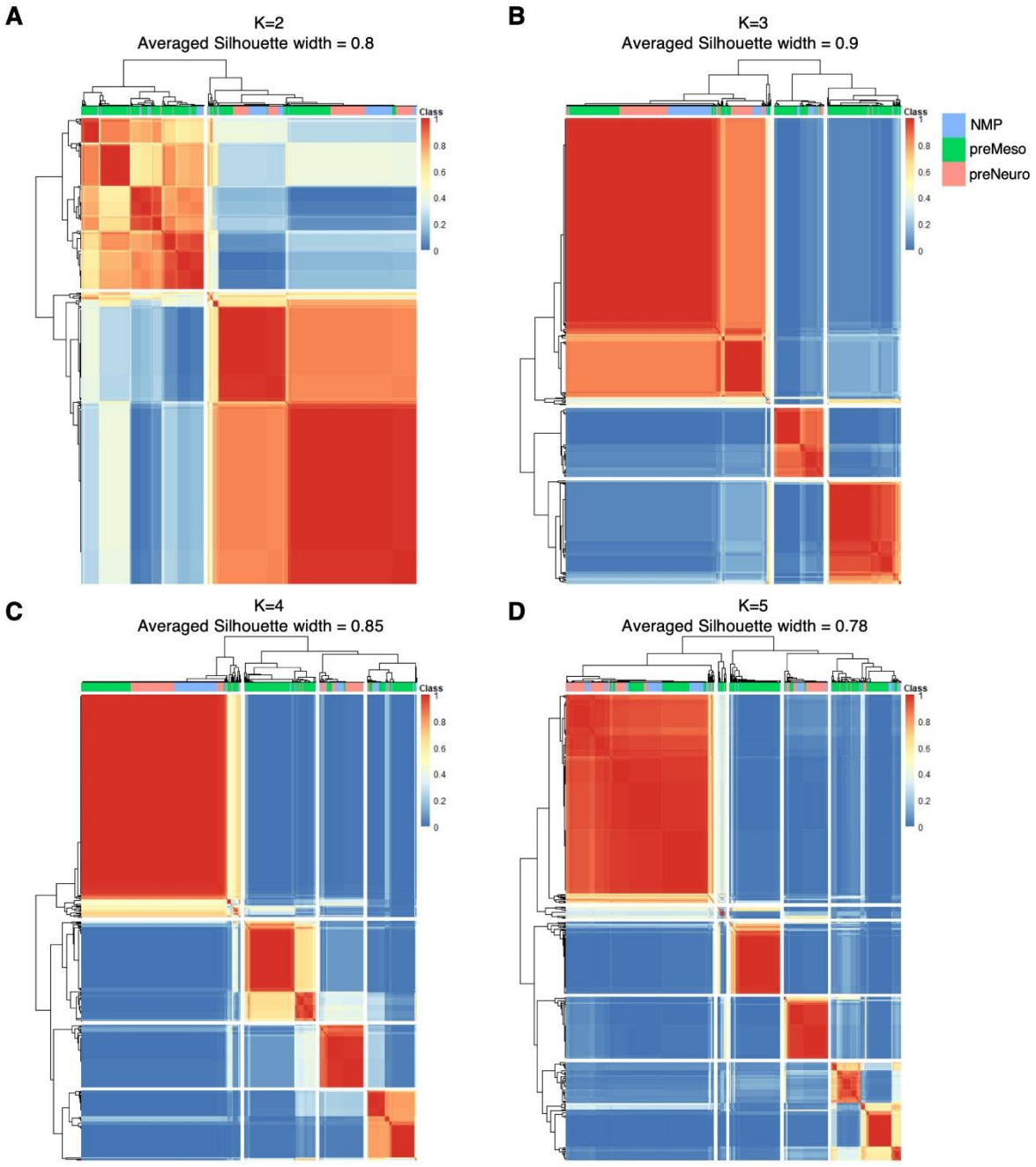

Figure S6. The averaged Silhouette width and the consensus matrices obtained for the embryo CLE for number of clusters: A. k = 2; **B.** k = 3; **C.** k = 4 and **D.** k = 5. Cells that were defined as NMP candidates, mesodermal progenitors (preMeso) and neural progenitors (preNeuro) are marked in blue, green and pink respectively.

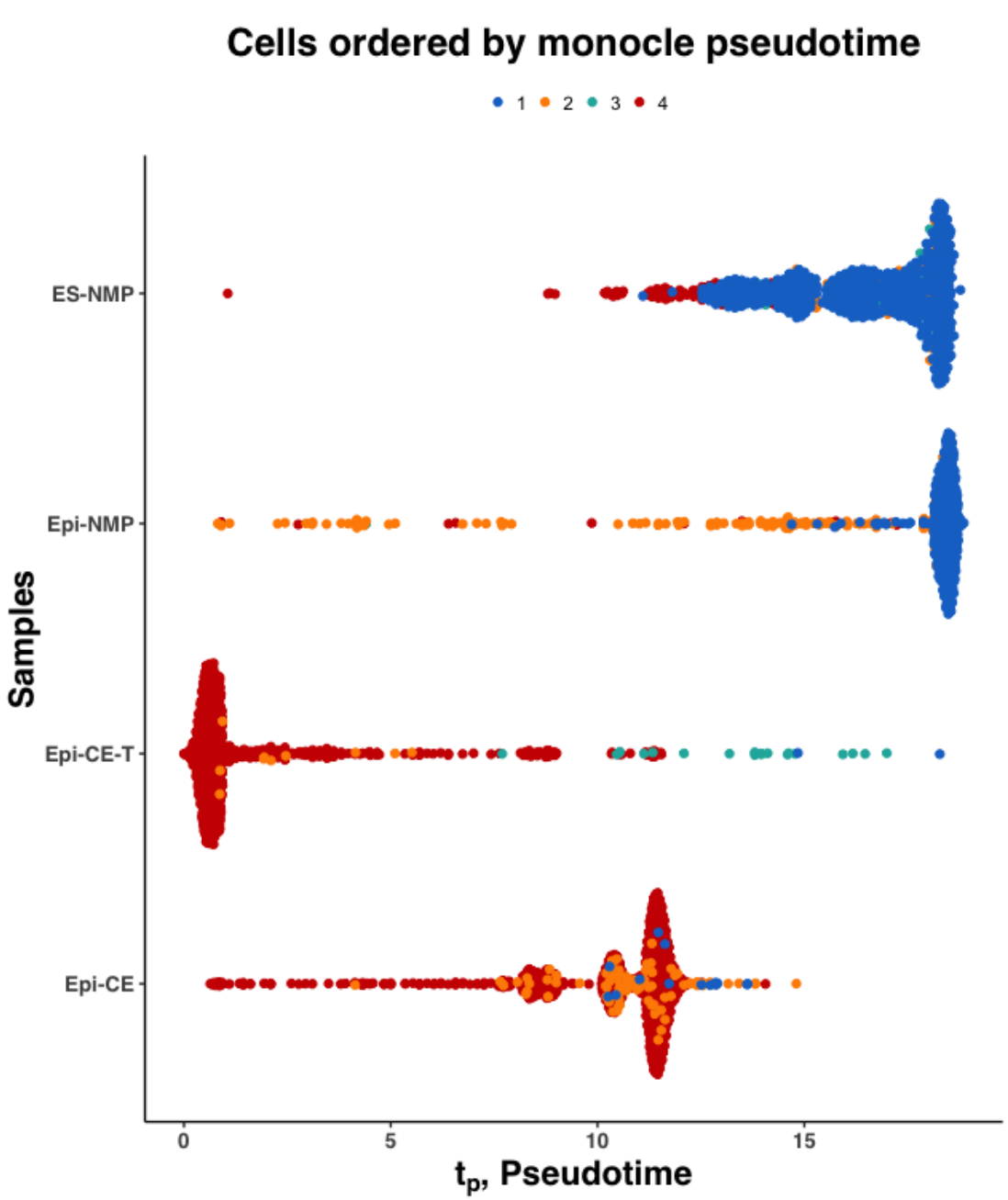

Figure S7. Monocle Pseudotemporal order of the *in vitro* cells. The cells are ordered along the pseudotime in the x-axis for every *in vitro* sample in the y-axis, where the cells that were classified to the 4 classes are coloured.

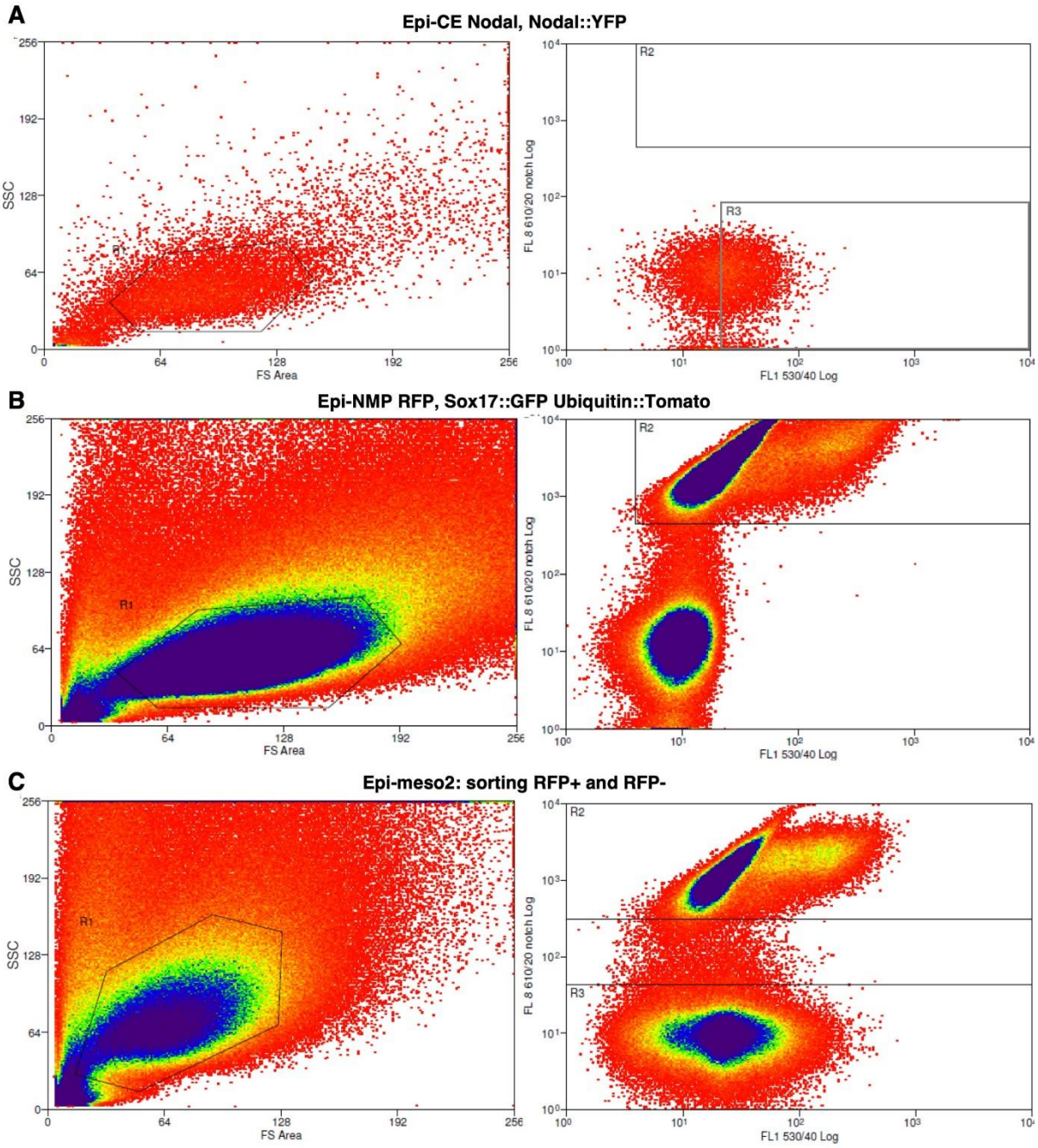

Figure S8. Node like cell with Epi-NMP mixture and sorting. Cells were sorted using a MoFlo sorter (Beckman Coulter). Single cells were collected according to the plot of SSC (side scattered light) versus FC (forward scattered light) Area (SSC versus FS area plots). The lasers that were used are 647nm laser with emission filter of 610/20 to collect the RFP positive cells and 488nm laser with emission filter of 530/40 to collect the YFP positive cells (FL8 610/20 versus FL1 530/40 log scale plots). **A.** Epi-CE Nodal sample composed of Nodal::YFP cells that were cultured under the Epi-CE protocol. Only the YFP positive cells (R3 rectangle) were used to make the mixture of Epi-meso2 (see Materials and Methods). **B.** Epi-NMP RFP sample composed of Sox17::GFP Ubiquitin::Tomato cells, were culture under the Epi-NMP protocol. Only the RFP positive cells (R2 rectangle) were used to make the Epi-meso2 mixture together with the Epi-CE Nodal YFP positive cells. **C**. After growing the mixture of Epi-meso2 for 4 days the cells were sorted based on their RFP fluorescence: RFP positive cells (R2 rectangle, sample named EM2-RFP+4d) and RFP negative cells (R3 rectangle, sample named EM2-RFP-4d). The sorted cells were quantified for their RNA of a chosen set of genes using RT-qPCR technique (Materials and Methods).

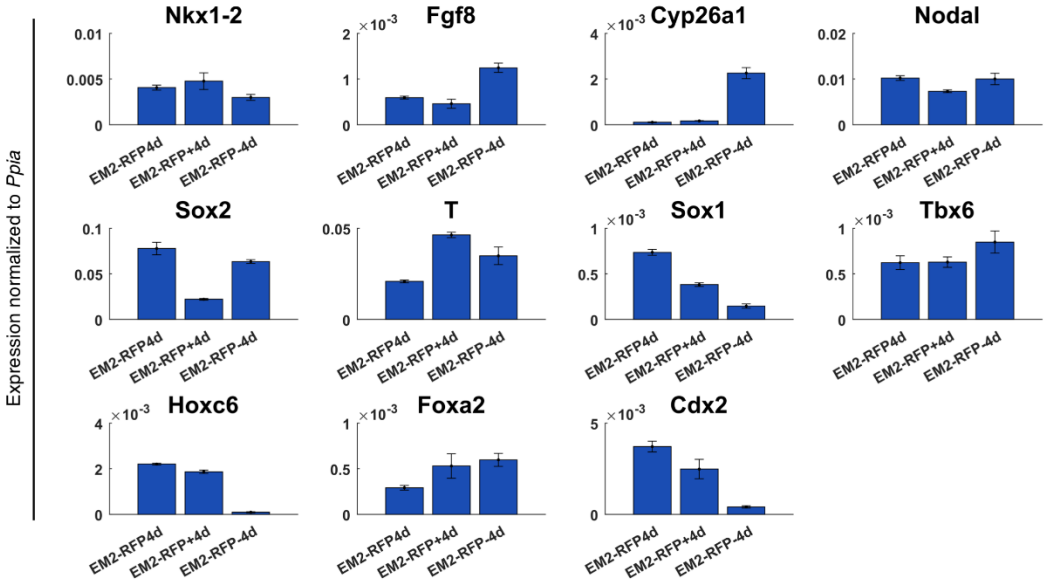

Figure S9. Gene expression of the sorted Epi-meso2 mixture and its control. The RNA expression of the sorted cells: EM2-RFP+4d and EM2-RFP-4d and the control sample EM2-RFP4d, was quantified for a chosen set of 11 genes using RT-qPCR technique. The bars represent the averaged gene expression normalized against the housekeeping gene *Ppia* across 3 technical replicas and the error bars indicate the standard deviation between the triplicates.

Reference

Acampora, D., Di Giovannantonio, L. G., Di Salvio, M., Mancuso, P. and Simeone, A. (2009). Selective inactivation of Otx2 mRNA isoforms reveals isoform-specific requirement for visceral endoderm anteriorization and head morphogenesis and highlights cell diversity in the visceral endoderm. *Mech. Dev.* **126**, 882–897.

Akiyama, H., Chaboissier, M.-C., Martin, J. F., Schedl, A. and de Crombrugghe, B. (2002). The transcription factor Sox9 has essential roles in successive steps of the chondrocyte differentiation pathway and is required for expression of Sox5 and Sox6. *Genes Dev.* **16**, 2813–28.

Anderson, W. J., Zhou, Q., Alcalde, V., Kaneko, O. F., Blank, L. J., Sherwood, R. I., Guseh, J. S., Rajagopal, J. and Melton, D. A. (2008). Genetic targeting of the endoderm with claudin-6CreER. *Dev. Dyn.* **237**, 504–512.

Bachler, M. and Neubüser, A. (2001). Expression of members of the Fgf family and their receptors during midfacial development. *Mech. Dev.* **100**, 313–316.

Bajanca, F., Luz, M., Duxson, M. J. and Thorsteinsdóttir, S. (2004). Integrins in the mouse myotome: Developmental changes and differences between the epaxial and hypaxial lineage. *Dev. Dyn.* **231**, 402–415.

Barrionuevo, F., Taketo, M. M., Scherer, G. and Kispert, A. (2006). Sox9 is required for notochord maintenance in mice. *Dev. Biol.* **295**, 128–140.

Basilicata, M. F., Frank, M., Solter, D., Brabletz, T. and Stemmler, M. P. (2016). Inappropriate cadherin switching in the mouse epiblast compromises proper signaling between the epiblast and the extraembryonic ectoderm during gastrulation. *Sci. Rep.* **6**, 26562.

Bel-Vialar, S., Medevielle, F. and Pituello, F. (2007). The on/off of Pax6 controls the tempo of neuronal differentiation in the developing spinal cord. *Dev. Biol.* **305**, 659–673.

Bessho, Y., Miyoshi, G., Sakata, R. and Kageyama, R. (2001a). Hes7: a bHLH-type repressor gene regulated by Notch and expressed in the presomitic mesoderm. *Genes to Cells* **6**, 175–185.

Bessho, Y., Sakata, R., Komatsu, S., Shiota, K., Yamada, S. and Kageyama, R. (2001b). Dynamic expression and essential functions of Hes7 in somite segmentation. *Genes Dev.* **15**, 2642–7.

Boyle, S., Shioda, T., Perantoni, A. O. and de Caestecker, M. (2007). Cited1 and Cited2 are differentially expressed in the developing kidney but are not required for nephrogenesis. *Dev. Dyn.* **236**, 2321–2330.

Cajal, M., Lawson, K. A., Hill, B., Moreau, A., Rao, J., Ross, A., Collignon, J., Camus, A., Simeone, A. and Levi, G. (2012). Clonal and molecular analysis of the prospective anterior neural boundary in the mouse embryo. *Development* **139**, 423–36.

Cambray, N. and Wilson, V. (2007). Two distinct sources for a population of maturing axial progenitors. *Development* **134**, 2829–2840.

Cano, A., Pérez-Moreno, M. A., Rodrigo, I., Locascio, A., Blanco, M. J., del Barrio, M. G., Portillo, F. and Nieto, M. A. (2000). The transcription factor Snail controls epithelial–mesenchymal transitions by repressing E-cadherin expression. *Nat. Cell Biol.* **2**, 76–83.

Carver, E. A., Jiang, R., Lan, Y., Oram, K. F. and Gridley, T. (2001). The mouse snail gene encodes a key regulator of the epithelial-mesenchymal transition. *Mol. Cell. Biol.* **21**, 8184–8.

Chalamalasetty, R. B., Dunty, W. C., Biris, K. K., Ajima, R., Iacovino, M., Beisaw, A., Feigenbaum, L., Chapman, D. L., Yoon, J. K., Kyba, M., et al. (2011). The Wnt3a/β-catenin target gene Mesogenin1 controls the segmentation clock by activating a Notch signalling program. *Nat. Commun.* **2**, 390.

Chalamalasetty, R. B., Garriock, R. J., Dunty, W. C., Kennedy, M. W., Jailwala, P., Si, H. and Yamaguchi, T. P. (2014). Mesogenin 1 is a master regulator of paraxial presomitic mesoderm differentiation. *Development* **141**, 4285–97.

Chambers, I., Colby, D., Robertson, M., Nichols, J., Lee, S., Tweedie, S. and Smith, A. (2003). Functional Expression Cloning of Nanog, a Pluripotency Sustaining Factor in Embryonic Stem Cells. *Cell* **113**, 643–655.

Chambers, I., Silva, J., Colby, D., Nichols, J., Nijmeijer, B., Robertson, M., Vrana, J., Jones, K., Grotewold, L. and Smith, A. (2007). Nanog safeguards pluripotency and mediates germline development. *Nature* **450**, 1230–1234.

Colbert, M. C., Rubin, W. W., Linney, E. and LaMantia, A.-S. (1995). Retinoid signaling and the generation of regional and cellular diversity in the embryonic mouse spinal cord. *Dev. Dyn.* **204**, 1–12.

Cooper, M. A., Crockett, D. P., Nowakowski, R. S., Gale, N. W. and Zhou, R. (2009). Distribution of EphA5 receptor protein in the developing and adult mouse nervous system. *J. Comp. Neurol.* **514**, 310–28.

Cunningham, T. J., Kumar, S., Yamaguchi, T. P. and Duester, G. (2015). Wnt8a and Wnt3a cooperate in the axial stem cell niche to promote mammalian body axis extension. *Dev. Dyn.* **244**, 797–807.

Cunningham, T. J., Colas, A. and Duester, G. (2016). Early molecular events during retinoic acid induced differentiation of neuromesodermal progenitors. *Biol. Open* **5**, bio.020891.

Danesh, S. M., Villasenor, A., Chong, D., Soukup, C. and Cleaver, O. (2009). BMP and BMP receptor expression during murine organogenesis. *Gene Expr. Patterns* **9**, 255–65.

Davies, O. R., Lin, C.-Y., Radzisheuskaya, A., Zhou, X., Taube, J., Blin, G., Waterhouse, A., Smith, A. J. H. and Lowell, S. (2013). Tcf15 primes pluripotent cells for differentiation. *Cell Rep.* **3**, 472–84.

De Vries, W. N., Evsikov, A. V, Haac, B. E., Fancher, K. S., Holbrook, A. E., Kemler, R., Solter, D. and Knowles, B. B. (2004). Maternal beta-catenin and E-cadherin in mouse development. *Development* **131**, 4435–45.

del Moral, P.-M., De Langhe, S. P., Sala, F. G., Veltmaat, J. M., Tefft, D., Wang, K., Warburton, D. and Bellusci, S. (2006). Differential role of FGF9 on epithelium and mesenchyme in mouse embryonic lung. *Dev. Biol.* **293**, 77–89.

Deng, M., Yang, H., Xie, X., Liang, G. and Gan, L. (2014). Comparative expression analysis of POU4F1, POU4F2 and ISL1 in developing mouse cochleovestibular ganglion neurons. *Gene Expr. Patterns* **15**, 31–7.

Deschamps, J. and van Nes, J. (2005). Developmental regulation of the Hox genes during axial morphogenesis in the mouse. *Development* **132**, 2931–42.

Downs, K. M. (2008). Systematic localization of Oct-3/4 to the gastrulating mouse conceptus suggests manifold roles in mammalian development. *Dev. Dyn.* **237**, 464–475.

Duester, G. (2008). Retinoic Acid Synthesis and Signaling during Early Organogenesis. *Cell* **134**, 921–931.

Dunty, W. C., Biris, K. K., Chalamalasetty, R. B., Taketo, M. M., Lewandoski, M. and Yamaguchi, T. P. (2008). Wnt3a/beta-catenin signaling controls posterior body development by coordinating mesoderm formation and segmentation. *Development* **135**, 85–94.

Dunty, W. C., Kennedy, M. W. L., Chalamalasetty, R. B., Campbell, K. and Yamaguchi, T. P. (2014). Transcriptional profiling of Wnt3a mutants identifies Sp transcription factors as essential effectors of the Wnt/β-catenin pathway in neuromesodermal stem cells. *PLoS One* **9**, e87018.

Dunwoodie, S. L., Rodriguez, T. A. and Beddington, R. S. P. (1998). Msg1 and Mrg1, founding members of a gene family, show distinct patterns of gene expression during mouse embryogenesis. *Mech. Dev.* **72**, 27–40.

Edri, S., Hayward, P., Baillie-Johnson, P., Steventon, B. and Martinez Arias, A. (2018). An Epiblast Stem Cell derived multipotent progenitor population for axial extension. *bioRxiv* 242461.

Festuccia, N., Osorno, R., Halbritter, F., Karwacki-Neisius, V., Navarro, P., Colby, D., Wong, F., Yates, A., Tomlinson, S. R. and Chambers, I. (2012). Esrrb is a direct Nanog target gene that can substitute for Nanog function in pluripotent cells. *Cell Stem Cell* **11**, 477–90.

Fischer, T., Faus-Kessler, T., Welzl, G., Simeone, A., Wurst, W. and Prakash, N. (2011). Fgf15-mediated control of neurogenic and proneural gene expression regulates dorsal midbrain neurogenesis. *Dev. Biol.* **350**, 496–510.

Fujisawa, H. and Kitsukawa, T. (1998). Receptors for collapsin/semaphorins. *Curr. Opin. Neurobiol.* **8**, 587–592.

Funk, M. C., Bera, A. N., Menchen, T., Kuales, G., Thriene, K., Lienkamp, S. S., Dengjel, J., Omran, H., Frank, M. and Arnold, S. J. (2015). Cyclin O (Ccno) functions during deuterosome-mediated centriole amplification of multiciliated cells. *EMBO J.* **34**, 1078–89.

Girós, A., Grgur, K., Gossler, A. and Costell, M. (2011). α5β1 Integrin-Mediated Adhesion to Fibronectin Is Required for Axis Elongation and Somitogenesis in Mice. *PLoS One* **6**, e22002.

Goulding, M. D., Chalepakis, G., Deutsch, U., Erselius, J. R. and Gruss, P. (1991). Pax-3, a novel murine DNA binding protein expressed during early neurogenesis. *EMBO J.* **10**, 1135–47.

Haghverdi, L., Lun, A. T. L., Morgan, M. D. and Marioni, J. C. (2018). Batch effects in single-cell RNA-sequencing data are corrected by matching mutual nearest neighbors. *Nat. Biotechnol.* **36**, 421–427.

Hagiwara, N. (2011). Sox6, jack of all trades: a versatile regulatory protein in vertebrate development. *Dev. Dyn.* **240**, 1311–21.

Hart, A. H., Hartley, L., Sourris, K., Stadler, E. S., Li, R., Stanley, E. G., Tam, P. P. L., Elefanty, A. G. and Robb, L. (2002). Mixl1 is required for axial mesendoderm

morphogenesis and patterning in the murine embryo. *Development* **129**, 3597–608.

Hebert, J. M., Boyle, M. and Martin, G. R. (1991). mRNA localization studies suggest that murine FGF-5 plays a role in gastrulation. *Development* **112**,.

Henrique, D., Abranches, E., Verrier, L. and Storey, K. G. (2015). Neuromesodermal progenitors and the making of the spinal cord. *Development* **142**, 2864–2875.

Hitoshi, S., Ishino, Y., Kumar, A., Jasmine, S., Tanaka, K. F., Kondo, T., Kato, S., Hosoya, T., Hotta, Y. and Ikenaka, K. (2011). Mammalian Gcm genes induce Hes5 expression by active DNA demethylation and induce neural stem cells. *Nat. Neurosci.* **14**, 957–964.

Hou, J., Charters, A. M., Lee, S. C., Zhao, Y., Wu, M. K., Jones, S. J., Marra, M. A. and Hoodless, P. A. (2007). A systematic screen for genes expressed in definitive endoderm by Serial Analysis of Gene Expression (SAGE). *BMC Dev. Biol.* **7**, 92.

Howe, C. C., Overton, G. C., Sawicki, J., Solter, D., Stein, P. and Strickland, S. (1988). Expression of SPARC/osteonectin transcript in murine embryos and gonads. *Differentiation* **37**, 20–25.

Ishii, M., Han, J., Yen, H.-Y., Sucov, H. M., Chai, Y. and Maxson, R. E. (2005). Combined deficiencies of Msx1 and Msx2 cause impaired patterning and survival of the cranial neural crest. *Development* **132**, 4937–50.

Jukkola, T., Trokovic, R., Maj, P., Lamberg, A., Mankoo, B., Pachnis, V., Savilahti, H. and Partanen, J. (2005). Meox1Cre: A mouse line expressing Cre recombinase in somitic mesoderm. *genesis* **43**, 148–153.

Khairallah, H., El Andalousi, J., Simard, A., Haddad, N., Chen, Y.-H., Hou, J., Ryan, A. K. and Gupta, I. R. (2014). Claudin-7, -16, and -19 during mouse kidney development. *Tissue barriers* **2**, e964547.

Khoa, L. T. P., Azami, T., Tsukiyama, T., Matsushita, J., Tsukiyama-Fujii, S., Takahashi, S. and Ema, M. (2016). Visualization of the Epiblast and Visceral Endodermal Cells Using Fgf5-P2A-Venus BAC Transgenic Mice and Epiblast Stem Cells. *PLoS One* **11**, e0159246.

Klymiuk, I., Kenner, L., Adler, T., Busch, D. H., Boersma, A., Irmler, M., Gailus-Durner, V., Fuchs, H., Leitner, N., Müller, M., et al. (2012). In Vivo Functional Requirement of the Mouse Ifitm1 Gene for Germ Cell Development, Interferon Mediated Immune Response and Somitogenesis. *PLoS One* **7**, e44609.

Kojima, Y., Kaufman-Francis, K., Studdert, J. B., Steiner, K. A., Power, M. D., Loebel, D. A. F., Jones, V., Hor, A., De Alencastro, G., Logan, G. J., et al. (2014). The transcriptional and functional properties of mouse epiblast stem cells resemble the anterior primitive streak. *Cell Stem Cell* **14**, 107–120.

Lan, Y., Liu, H., Ovitt, C. E. and Jiang, R. (2011). Generation of Osr1 conditional mutant mice. *Genesis* **49**, 419–22.

Lange, U. C., Saitou, M., Western, P. S., Barton, S. C. and Surani, M. A. (2003). The fragilis interferon-inducible gene family of transmembrane proteins is associated with germ cell specification in mice. *BMC Dev. Biol.* **3**, 1.

Lawson, K. A., Dunn, N. R., Roelen, B. A., Zeinstra, L. M., Davis, A. M., Wright, C. V, Korving, J. P. and Hogan, B. L. (1999). Bmp4 is required for the generation of primordial germ cells in the mouse embryo. *Genes Dev.* **13**, 424–36.

Lee, S.-J., McPherron, A. C. and Lawler, A. M. (1999). Regulation of anterior/posterior patterning of the axial skeleton by growth/differentiation factor 11. *Nat. Genet.* **22**, 260–264.

Lefebvre, L. (2012). The placental imprintome and imprinted gene function in the trophoblast glycogen cell lineage. *Reprod. Biomed. Online* **25**, 44–57.

Lobe, C. G. (1997). Expression of the helix-loop-helix factor, Hes3, during embryo development suggests a role in early midbrain-hindbrain patterning. *Mech. Dev.* **62**, 227–237.

Lu, C. C. and Robertson, E. J. (2004). Multiple roles for Nodal in the epiblast of the mouse embryo in the establishment of anterior-posterior patterning. *Dev. Biol.* **273**, 149–159.

Maruoka, Y., Ohbayashi, N., Hoshikawa, M., Itoh, N., Hogan, B. L. M. and Furuta, Y. (1998). Comparison of the expression of three highly related genes, Fgf8, Fgf17 and Fgf18, in the mouse embryo. *Mech. Dev.* **74**, 175–177.

Maruyama, M., Ichisaka, T., Nakagawa, M. and Yamanaka, S. (2005). Differential roles for Sox15 and Sox2 in transcriptional control in mouse embryonic stem cells. *J. Biol. Chem.* **280**, 24371–9.

Maskell, L. J., Qamar, K., Babakr, A. A., Hawkins, T. A., Heads, R. J. and Budhram-Mahadeo, V. S. (2017). Essential but partially redundant roles for POU4F1/Brn-3a and POU4F2/Brn-3b transcription factors in the developing heart. *Cell Death Dis.* **8**, e2861.

Maurer, J., Nelson, B., Ceceña, G., Bajpai, R., Mercola, M., Terskikh, A. and Oshima, R. G. (2008). Contrasting Expression of Keratins in Mouse and Human Embryonic Stem Cells. *PLoS One* **3**, e3451.

Myers, P. (2008). Hox Genes in Development: The Hox Code. *Nature*.

Nagai, T., Aruga, J., Takada, S., Günther, T., Spörle, R., Schughart, K. and Mikoshiba, K. (1997). The Expression of the MouseZic1, Zic2,andZic3Gene Suggests an Essential Role forZicGenes in Body Pattern Formation. *Dev. Biol.* **182**, 299–313.

Niswander, L. and Martin, G. R. (1992). Fgf-4 expression during gastrulation, myogenesis, limb and tooth development in the mouse. *Development* **114**,.

Papp, B. and Plath, K. (2012). Pluripotency re-centered around Esrrb. *EMBO J.* **31**, 4255–7.

Parr Brian A., Shea Martin J., Vassileva Galya and McMahon Andrew P. (1993). Mouse Wnt genes exhibit discrete domains of expression in the early embryonic CNS and limb buds. *Development* **119**, 247–261.

Pearce, J. J. H. and Evans, M. J. (1999). Mml, a mouse Mix-like gene expressed in the primitive streak. *Mech. Dev.* **87**, 189–192.

Pevny, L. H., Sockanathan, S., Placzek, M. and Lovell-Badge, R. (1998). A role for SOX1 in neural determination. *Development* **125**,.

Pontecorvi, M., Goding, C. R., Richardson, W. D. and Kessaris, N. (2008). Expression of Tbx2 and Tbx3 in the developing hypothalamic–pituitary axis. *Gene Expr. Patterns* **8**, 411–417.

Redmer, T., Diecke, S., Grigoryan, T., Quiroga-Negreira, A., Birchmeier, W. and Besser, D. (2011). E-cadherin is crucial for embryonic stem cell pluripotency and can replace OCT4 during somatic cell reprogramming. *EMBO Rep.* **12**, 720–6.

Relaix, F., Rocancourt, D., Mansouri, A. and Buckingham, M. (2004). Divergent

functions of murine Pax3 and Pax7 in limb muscle development. *Genes Dev.* **18**, 1088–105.

Robb, L., Hartley, L., Begley, C. G., Brodnicki, T. C., Copeland, N. G., Gilbert, D. J., Jenkins, N. A. and Elefanty, A. G. (2000). Cloning, expression analysis, and chromosomal localization of murine and human homologues of aXenopus Mix gene. *Dev. Dyn.* **219**, 497–504.

Rodriguez, T. A., Sparrow, D. B., Scott, A. N., Withington, S. L., Preis, J. I., Michalicek, J., Clements, M., Tsang, T. E., Shioda, T., Beddington, R. S. P., et al. (2004). Cited1 is required in trophoblasts for placental development and for embryo growth and survival. *Mol. Cell. Biol.* **24**, 228–44.

Rosenfield, S. M., Bowden, E. T., Cohen-Missner, S., Gibby, K. A., Ory, V., Henke, R. T., Riegel, A. T. and Wellstein, A. (2012). Pleiotrophin (PTN) expression and function and in the mouse mammary gland and mammary epithelial cells. *PLoS One* **7**, e47876.

Russell, R., Ilg, M., Lin, Q., Wu, G., Lechel, A., Bergmann, W., Eiseler, T., Linta, L., Kumar P, P., Klingenstein, M., et al. (2015). A Dynamic Role of TBX3 in the Pluripotency Circuitry. *Stem cell reports* **5**, 1155–1170.

Saga, Y., Hata, N., Kobayashi, S., Magnuson, T., Seldin, M. F. and Taketo, M. M. (1996). MesP1: a novel basic helix-loop-helix protein expressed in the nascent mesodermal cells during mouse gastrulation. *Development* **122**,.

Saga, Y., Hata, N., Koseki, H. and Taketo, M. M. (1997). Mesp2: a novel mouse gene expressed in the presegmented mesoderm and essential for segmentation initiation. *Genes Dev.* **11**, 1827–39.

Sakai, Y., Meno, C., Fujii, H., Nishino, J., Shiratori, H., Saijoh, Y., Rossant, J. and Hamada, H. (2001). The retinoic acid-inactivating enzyme CYP26 is essential for establishing an uneven distribution of retinoic acid along the anterio-posterior axis within the mouse embryo. *Genes Dev.* **15**, 213–25.

Schubert, F. R., Fainsod, A., Gruenbaum, Y. and Gruss, P. (1995). Expression of the novel murine homeobox gene Sax-1 in the developing nervous system. *Mech. Dev.* **51**, 99–114.

Schwarz, Q., Maden, C. H., Vieira, J. M. and Ruhrberg, C. (2009). Neuropilin 1 signaling guides neural crest cells to coordinate pathway choice with cell specification. *Proc. Natl. Acad. Sci. U. S. A.* **106**, 6164–9.

Shi, G. and Jin, Y. (2010). Role of Oct4 in maintaining and regaining stem cell pluripotency. *Stem Cell Res. Ther.* **1**, 39.

Sirbu, I. O. and Duester, G. (2006). Retinoic-acid signalling in node ectoderm and posterior neural plate directs left–right patterning of somitic mesoderm. *Nat. Cell Biol.* **8**, 271–277.

Stuckey, D. W., Di Gregorio, A., Clements, M. and Rodriguez, T. A. (2011). Correct Patterning of the Primitive Streak Requires the Anterior Visceral Endoderm. *PLoS One* **6**, e17620.

Sun, X., Meyers, E. N., Lewandoski, M. and Martin, G. R. (1999). Targeted disruption of Fgf8 causes failure of cell migration in the gastrulating mouse embryo. *Genes Dev.* **13**, 1834–46.

Sun, J., Ting, M.-C., Ishii, M. and Maxson, R. (2016). Msx1 and Msx2 function together in

the regulation of primordial germ cell migration in the mouse. *Dev. Biol.* **417**, 11–24.

Tortelote, G. G., Hernández-Hernández, J. M., Quaresma, A. J. C., Nickerson, J. A., Imbalzano, A. N. and Rivera-Pérez, J. A. (2013). Wnt3 function in the epiblast is required for the maintenance but not the initiation of gastrulation in mice. *Dev. Biol.* **374**, 164–73.

Toyooka, Y., Shimosato, D., Murakami, K., Takahashi, K. and Niwa, H. (2008). Identification and characterization of subpopulations in undifferentiated ES cell culture. *Development* **135**, 909–18.

Tsuda, M., Sasaoka, Y., Kiso, M., Abe, K., Haraguchi, S., Kobayashi, S. and Saga, Y. (2003). Conserved Role of nanos Proteins in Germ Cell Development. *Science (80-.).* **301**, 1239–1241.

Wahl, M. B., Deng, C., Lewandoski, M. and Pourquié, O. (2007). FGF signaling acts upstream of the NOTCH and WNT signaling pathways to control segmentation clock oscillations in mouse somitogenesis. *Development* **134**, 4033–41.

Wang, Q., Lan, Y., Cho, E.-S., Maltby, K. M. and Jiang, R. (2005). Odd-skipped related 1 (Odd1) is an essential regulator of heart and urogenital development. *Dev. Biol.* **288**, 582–594.

Wang, B., Ye, T.-M., Lee, K.-F., Chiu, P. C. N., Pang, R. T. K., Ng, E. H. Y. and Yeung, W. S. B. (2015). Annexin A2 Acts as an Adhesion Molecule on the Endometrial Epithelium during Implantation in Mice. *PLoS One* **10**, e0139506.

Weinreb, C., Wolock, S. and Klein, A. M. (2017). SPRING: a kinetic interface for visualizing high dimensional single-cell expression data. *Bioinformatics*.

White, P. H., Farkas, D. R., McFadden, E. E. and Chapman, D. L. (2003). Defective somite patterning in mouse embryos with reduced levels of Tbx6. *Development* **130**, 1681–90.

Wolfe, A. D. and Downs, K. M. (2014). Mixl1 localizes to putative axial stem cell reservoirs and their posterior descendants in the mouse embryo. *Gene Expr. Patterns* **15**, 8–20.

Wood, H. B. and Episkopou, V. (1999). Comparative expression of the mouse Sox1, Sox2 and Sox3 genes from pre-gastrulation to early somite stages. *Mech. Dev.* **86**, 197–201.

Wright, E., Hargrave, M. R., Christiansen, J., Cooper, L., Kun, J., Evans, T., Gangadharan, U., Greenfield, A. and Koopman, P. (1995). The Sry-related gene Sox9 is expressed during chondrogenesis in mouse embryos. *Nat. Genet.* **9**, 15–20.

Wright, T. J., Hatch, E. P., Karabagli, H., Karabagli, P., Schoenwolf, G. C. and Mansour, S. L. (2003). Expression of mouse fibroblast growth factor and fibroblast growth factor receptor genes during early inner ear development. *Dev. Dyn.* **228**, 267–272.

Yamaguchi, T. P., Bradley, A., McMahon, A. P. and Jones, S. (1999). A Wnt5a pathway underlies outgrowth of multiple structures in the vertebrate embryo. *Development* **126**, 1211–1223.

Zakin, L. and De Robertis, E. M. (2004). Inactivation of mouse Twisted gastrulation reveals its role in promoting Bmp4 activity during forebrain development. *Development* **131**, 413–24.

Zhao, T., Zhou, X., Szabó, N., Leitges, M. and Alvarez-Bolado, G. (2007). Foxb1-drivenCre expression in somites and the neuroepithelium of diencephalon, brainstem,

and spinal cord. *genesis* **45**, 781–787.

Zhu, Q., Song, L., Peng, G., Sun, N., Chen, J., Zhang, T., Sheng, N., Tang, W., Qian, C., Qiao, Y., et al. (2014). The transcription factor Pou3f1 promotes neural fate commitment via activation of neural lineage genes and inhibition of external signaling pathways. *Elife* **3**,.